Pion generalized parton distributions with covariant and light-front constituent quark models

T. Frederico,[1] E. Pace,[2] B. Pasquini,[3] and G. Salmè[4]

[1]*Departamento de Física, Instituto Tecnológico de Aeronáutica, 12.228-900 São José dos Campos, São Paulo, Brazil*
[2]*Dipartimento di Fisica, Università di Roma, "Tor Vergata" and Istituto Nazionale di Fisica Nucleare, Sezione Tor Vergata, Via della Ricerca Scientifica 1, I-00133 Roma, Italy*
[3]*Dipartimento di Fisica Nucleare e Teorica, Università degli Studi di Pavia and Istituto Nazionale di Fisica Nucleare, Sezione di Pavia, Italy*
[4]*Istituto Nazionale di Fisica Nucleare, Sezione di Roma, Piazzale A. Moro 2, I-00185 Roma, Italy*

(Received 31 July 2009; published 23 September 2009)

We investigate the model dependence of no-helicity flip generalized parton distribution of the pion upon different approaches for the quark-hadron and quark-photon vertices, in the spacelike region. In order to obtain information on contributions from both the valence and the nonvalence regions, we compare results for spacelike momentum transfers obtained from (i) an analytic covariant model with a bare quark-photon vertex, (ii) a light-front approach with a quark-photon vertex dressed through a microscopic vector-meson model, and (iii) a light-front approach based on the relativistic Hamiltonian dynamics. Our comparisons lead us to infer the same dynamical mechanism, the one-gluon-exchange dominance at short distances, as a source of both the electromagnetic form factor at large momentum transfer and the parton distribution close to the end points. The expected collinear behavior of the generalized parton distributions at high-momentum transfer, i.e. a maximum for $x \sim 1$, is also illustrated, independently of the different approaches. Finally, a comparison with recent lattice calculations of the gravitational form factors is presented.

DOI: 10.1103/PhysRevD.80.054021 PACS numbers: 12.39.Ki, 11.10.St, 13.40.−f, 14.40.Aq

I. INTRODUCTION

In recent years, a growing interest in the study of the deeply virtual Compton scattering (DVCS) has motivated an impressive amount of work aimed at the extraction of the so-called generalized parton distributions (GPDs) from experimental data (see, e.g., Refs. [1–6] for recent reviews). In principle, GPDs allow one to achieve an unprecedented level of detail on the knowledge of hadronic states.

Naturally, the pion GPD should represent a test ground of any approach that addresses the issue of obtaining a detailed description of hadron structure, and this explains the wealth of papers devoted to such a task (see, e.g., [4,7–16]). In what follows, we focus on the GPDs that do not depend upon the helicities of the constituents; namely, we analyze the pion isoscalar and isovector GPDs, as defined, e.g., in [12].

The aim of our paper is the investigation of the model dependence of those no-helicity flip (chiral-even) GPDs of the pion upon different relativistic approaches in the spacelike region, i.e. for negative values of $t = (p' - p)^2$, where p and p' are the initial and final four-momenta of the pion, respectively. In particular, the study of the GPDs in the valence and nonvalence regions (see the following section) is emphasized by the choice of three different models that explore different kinematical regions: (i) a covariant analytic constituent quark (CQ) model that covers the whole kinematical domain and allows us to interpolate between the other two models; (ii) two phenomenological models, elaborated within a light-front (LF) framework (see, e.g., [17–19] for a review), which have a smaller kinematical range of applicability; namely, one addresses the nonvalence region and the other the valence one.

The first model is analytic and covariant and depends upon the mass of the constituents and a parameter, fixed by the decay constant of the pion. The main ingredients of such an approach are (i) the Bethe-Salpeter amplitude (BSA) of the pion, modeled through an analytic ansatz in the Minkowski space, (ii) the Mandelstam formula [20] (or impulse approximation formula) for the matrix elements of the current operator, and (iii) a bare quark-photon vertex. A peculiar feature of our ansatz for the pion BSA is given by the symmetry under the exchange of the constituent momenta. The first version of such a model was adopted in Ref. [21] to investigate the frame dependence of the description of the electromagnetic (em) pion form factor, putting in evidence the possibility to study the nonvalence content of the pion by using a suitable reference frame. In the present work, we consider a natural extension of the model that features a better end-point behavior of the BSA, as well.

A second model, developed within the LF dynamics and already applied to the em pion form factor in both the space- and timelike regions [22], is still based on the Mandelstam formula. However, this model retains only the analytic structure given by the poles of the Dirac propagators in the analytic integration over $k^- = k^0 - k^3$, i.e. the minus component of the constituent four-momentum appearing in the loop formula. An important consequence of the k^- integration can be reached in a

frame where the plus component of the virtual-photon four-momentum is different from zero, i.e. $\Delta^+ = \Delta^0 + \Delta^3 \neq 0$. Indeed, in this frame the contributions in the valence and nonvalence regions can be obtained, allowing an investigation of the Fock components of the hadronic state (see [4,18,19,23,24] for an overview of the Fock expansion of a hadron state, within the LF framework). Another relevant feature of this model, that has a fundamental impact in the timelike region, is the quark-photon vertex dressed by a microscopic version of the vector-meson model (VMD) [22]. Finally, as explained in detail in Ref. [22], the model lives in the nonvalence region, in the limit of vanishing pion mass.

A third model is constructed within the LF relativistic Hamiltonian dynamics (LFHD), where the Poincaré covariance is fully satisfied (see, e.g., [17] for a detailed review). In particular, the rotational covariance is fulfilled through the introduction of the Melosh rotations and the proper definition of the total intrinsic angular momentum. At the present stage, the model explores only the valence region.

The paper is organized as follows: In Sec. II, a brief résumé of the general properties of the pion isospin-dependent GPDs is presented; in Sec. III, the Fock decomposition of the GPDs is discussed, in view of a frame-dependent analysis; in Sec. IV, a covariant CQ model that allows an analytic evaluation of the pion GPDs is described; in Sec. V A, a first CQ light-front model, with a quark-photon vertex dressed by a microscopic version of the vector-meson dominance model, is presented; in Sec. V B, the LFHD model, where the full Poincaré covariance is implemented, is described. Finally, in Secs. VI and VII, the results are discussed and the conclusions drawn.

II. PION GPDS: KINEMATICS AND GENERAL FORMALISM

In the spacelike region, let us first illustrate the kinematics of the DVCS process with the symmetric momenta convention shown in Fig. 1 (see [13] for the reduction of the DVCS diagram to the one presented in Fig. 1, and the pioneering paper [25] for the deep inelastic scattering regime). For on-mass-shell pions, i.e. $p'^2 = p^2 = m_\pi^2$, and adopting standard notations (see, e.g., [4,6])

$$
\begin{aligned}
&t = \Delta^2 = (p' - p)^2,\\
&\xi = -\frac{\Delta \cdot n}{2P \cdot n} = -\frac{\Delta^+}{2P^+} = \frac{p^+ - p'^+}{p^+ + p'^+}, \qquad (|\xi| \leq 1),\\
&x = \frac{k \cdot n}{P \cdot n} = \frac{k^+}{P^+}, \qquad (1 \geq x \geq -1),
\end{aligned} \tag{1}
$$

where n is a lightlike four-vector, such that $v^+ = n \cdot v = v^0 + v^3$ [the scalar product is defined as $a \cdot b = (a^+ b^- + a^- b^+)/2 - \mathbf{a}_\perp \cdot \mathbf{b}_\perp$], $P = \frac{1}{2}(p' + p)$, and k is the average momentum of the active quark, i.e. the one that interacts with the photon (see Fig. 1). Notice that p^+ and p'^+ are necessarily positive, while $\Delta^+ \geq 0$ is taken by choice. From Eq. (1) one can trivially obtain the following useful relations:

$$
p'^+ = \frac{\Delta^+}{2}\left(1 - \frac{1}{\xi}\right), \qquad p^+ = -\frac{\Delta^+}{2}\left(1 + \frac{1}{\xi}\right). \tag{2}
$$

As is well known, the variable x allows one to single out (i) the valence region (where one has only contributions diagonal in the Fock space; cf. the following Sec. III) given by the union of two intervals $x \in [-1, -|\xi|]$ (corresponding to an active antiquark) and $x \in [|\xi|, 1]$ (corresponding to an active quark) and (ii) the nonvalence region $x \in [-|\xi|, |\xi|]$. Figure 2(a), shows a representative of the contribution with an active quark in the kinematical region $x \in [|\xi|, 1]$ (all of the constituents have a plus component of their own momentum bounded from above by the corresponding quantity of the parent pion). In Fig. 2(b), a contribution is shown from a pair-production process, nondiagonal in the Fock space. In Appendix A, a more detailed kinematical discussion is given. Finally, as a short detour, let us remind the reader that the pion BSA, integrated over the minus component of the quark momentum, yields the two-body Fock contribution to the pion state, notably nonvanishing only in the valence sector (see [19]).

Within the QCD-evolution framework, the valence region is called the Dokshitzer-Gribov-Lipatov-Altarelli-Parisi (DGLAP) [26] region, while the nonvalence one is called the Efremov-Radyushkin-Brodsky-Lepage (ERBL) [27,28] region.

In the interval $[|\xi|, 1]$, the relation between the LF momentum fraction x_q of the active constituent in the initial pion (with the support $[0, 1]$) and the variable x defined in Eq. (1) is given by

$$
x_q = \frac{k^+ - \Delta^+/2}{p^+} = \frac{k^+ - \Delta^+/2}{P^+ - \Delta^+/2} = \frac{x + \xi}{1 + \xi} = \frac{x - |\xi|}{1 - |\xi|}. \tag{3}
$$

The isospin-dependent GPDs (see, e.g., [4,7,12,14]) are the matrix elements of light-cone bilocal operators separated by a lightlike distance, $z^2 = z^+ z^- - |\mathbf{z}_\perp|^2 = 0$, evaluated between pion states with different initial and final

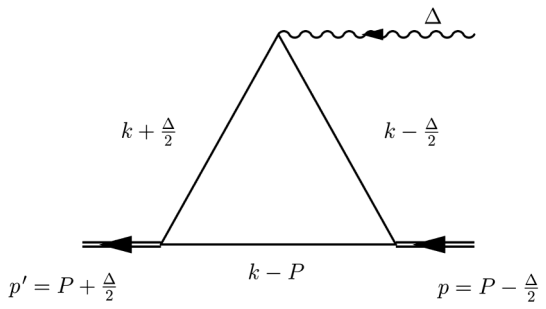

FIG. 1. Diagrammatic representation of the pion GPD, with four-momenta definitions.

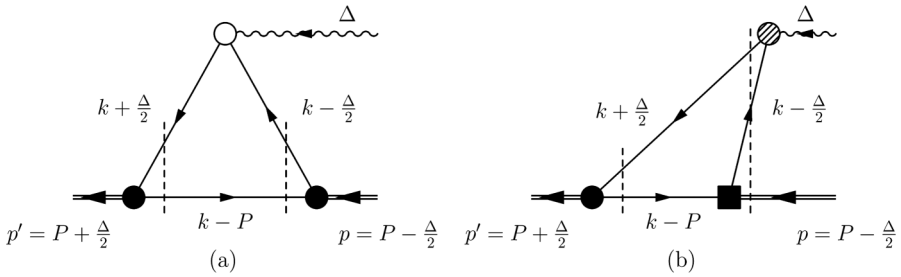

FIG. 2. LF time-ordered analysis of the pion GPD. Diagram (a) A contribution in the valence region, $1 \geq x \geq |\xi|$ (see text). Diagram (b) A contribution in the nonvalence region, $|\xi| > x > -|\xi|$ (see text). The vertical dashed lines indicate a given value of the LF time, in order to single out the number of constituents in flight.

momenta. In the light-cone gauge, where $A_{\rm gluon} \cdot n = 0$ and the gauge link becomes unity, one can introduce isoscalar and isovector combinations for the off-forward ($t \neq 0$), nondiagonal ($\xi \neq 0$) GPDs, as follows:

$$\begin{aligned} H^{I=0}_{\pi^\pm}(x,\xi,t) &= \int \frac{dz^-}{4\pi} e^{ixP^+z^-} \langle \pi^\pm(p')|\bar\psi_q\Big(-\frac{1}{2}z\Big) \\ &\quad \times \gamma\cdot n \psi_q\Big(\frac{1}{2}z\Big)|\pi^\pm(p)\rangle|_{\tilde z=0} \\ &= \frac{1}{2}[H^u_{\pi^+}(x,\xi,t) + H^d_{\pi^+}(x,\xi,t)] \\ &= \frac{1}{2}[H^d_{\pi^-}(x,\xi,t) + H^u_{\pi^-}(x,\xi,t)] \end{aligned} \tag{4}$$

and

$$\begin{aligned} H^{I=1}_{\pi^\pm}(x,\xi,t) &= \int \frac{dz^-}{4\pi} e^{ixP^+z^-} \langle \pi^\pm(p')|\bar\psi_q\Big(-\frac{1}{2}z\Big) \\ &\quad \times \gamma\cdot n \tau_3 \psi_q\Big(\frac{1}{2}z\Big)|\pi^\pm(p)\rangle|_{\tilde z=0} \\ &= \frac{1}{2}[H^u_{\pi^\pm}(x,\xi,t) - H^d_{\pi^\pm}(x,\xi,t)] \\ &= \pm\frac{1}{2}[H^u_{\pi^+}(x,\xi,t) - H^d_{\pi^+}(x,\xi,t)], \end{aligned} \tag{5}$$

where $\tilde z \equiv \{z^+, \boldsymbol{z}_\perp\}$, while $\psi_q(z)$ and $\tau_3\psi_q(z)$ are the following doublets of quark fields:

$$\begin{pmatrix} U(z) \\ D(z) \end{pmatrix}, \qquad \begin{pmatrix} U(z) \\ -D(z) \end{pmatrix}, \tag{6}$$

respectively. In Eqs. (4) and (5), following [7], instead of the Cartesian components π^0, π^1, and π^2 (adopted in [4,12,14]), the charged pions have been introduced, viz.,

$$|\pi^\pm\rangle = \frac{|\pi^1\rangle \pm i|\pi^2\rangle}{\sqrt{2}}, \qquad |\pi^0\rangle = |\pi^3\rangle. \tag{7}$$

The functions $H^u(x,\xi,t)$ and $H^d(x,\xi,t)$ are u and d GPDs, respectively, and contain quark and antiquark contributions (cf. the parton interpretation of H^q, e.g., in [1,4] and Fig. 2). It is worth noting that $H^q(x,\xi,t)$ has the support $x \in [-1,1]$. Finally, due to the isospin symmetry, one has

$$H^u_{\pi^+} = H^d_{\pi^-}, \tag{8}$$

and combining charge and isospin symmetry (G parity) one gets

$$H^u_{\pi^+}(x,\xi,t) = -H^u_{\pi^-}(-x,\xi,t) = -H^d_{\pi^+}(-x,\xi,t). \tag{9}$$

In what follows, we deal with a charged pion, and the subscript π^+ in the quark GPDs is dropped out whenever no ambiguity is present.

For vanishing ξ and t, one has the following partonic decomposition (cf. [1,4]):

$$\begin{aligned} H^u(x,0,0) &= \theta(x)u(x) - \theta(-x)\bar u(-x), \\ H^d(x,0,0) &= \theta(x)d(x) - \theta(-x)\bar d(-x). \end{aligned} \tag{10}$$

Equations (8) and (9) together with the partonic interpretation lead to the well known relations between the standard parton distribution functions (let us remind the reader that the relations pertain to active quarks), viz.,

$$u_{\pi^+}(x) = d_{\pi^-}(x), \qquad u_{\pi^+}(x) = \bar d_{\pi^+}(x). \tag{11}$$

The symmetry property of $H^{I=0,1}(x,\xi,t)$ (see, e.g., [4,7]) under the transformation $x \to -x$, that just reflects (i) the charge conjugation ($p \to -p$ and $p' \to -p'$) and (ii) the isospin invariance, reads [recalling Eqs. (8) and (9)]

$$\begin{aligned} H^{I=0}(x,\xi,t) &= \tfrac{1}{2}[H^u(x,\xi,t) - H^u(-x,\xi,t)] \\ &= -H^{I=0}(-x,\xi,t), \end{aligned} \tag{12}$$

$$\begin{aligned} H^{I=1}(x,\xi,t) &= \tfrac{1}{2}[H^u(x,\xi,t) + H^u(-x,\xi,t)] \\ &= H^{I=1}(-x,\xi,t). \end{aligned} \tag{13}$$

Therefore the two GPDs are odd or even in x depending upon the isospin combination. In addition, under the transformation $\xi \to -\xi$, that amounts to apply a time-reversal transformation (since we have to exchange the initial and final pion momenta) and to exploit Hermiticity, one has (see, e.g., [4,7])

$$H^I(x,\xi,t) = H^I(x,-\xi,t); \tag{14}$$

namely, $H^I(x,\xi,t)$ must be even in ξ.

From Eqs. (4) and (5) one has

$$H^u(x,\xi,t) = H^{I=0}(x,\xi,t) + H^{I=1}(x,\xi,t),$$
$$H^d(x,\xi,t) = H^{I=0}(x,\xi,t) - H^{I=1}(x,\xi,t). \quad (15)$$

As is well known, the following sum rules hold [note a different overall factor with respect to Refs. [12,14] due to our choice of dealing with a charged pion; cf. Eq. (7)]:

$$\int_{-1}^{1} dx H^{I=1}(x,\xi,t) = \int_{-1}^{1} dx H^u(x,\xi,t) = F_\pi(t), \quad (16)$$

$$\int_{-1}^{1} dx x H^{I=0}(x,\xi,t) = \int_{-1}^{1} dx x H^u(x,\xi,t) = \frac{1}{2}[\theta_2(t) - \xi^2\theta_1(t)]. \quad (17)$$

In Eq. (16), $F_\pi(t)$ is the pion em form factor (see Appendix C), while, according to Ref. [29], in Eq. (17), $\theta_1(t)$ and $\theta_2(t)$ are the gravitational form factors (see also, e.g., [7,12,15]) that enter in the parametrization of the matrix elements of the quark part of the energy-momentum tensor [notice that in the chiral limit one has $\theta_1(0) - \theta_2(0) = \mathcal{O}(m_\pi^2)$]. It should be pointed out that the sum rule (17) for $t = 0$ and $\xi = 0$ yields the longitudinal-momentum sum rule for the pion, i.e. $\langle x_q \rangle$, as numerically illustrated in Sec. VI.

For vanishing ξ and t, one can exploit (i) Eqs. (12) and (13) and (ii) the partonic decomposition [cf. Eq. (10)] obtaining

$$\begin{aligned} H^{I=0}(x,0,0) &= \tfrac{1}{2}[H^u(x,0,0) + H^d(x,0,0)] \\ &= \tfrac{1}{2}[H^u(x,0,0) - H^u(-x,0,0)] \\ &= \theta(x)\tfrac{1}{2}[u(x) + \bar{u}(x)] \\ &\quad - \theta(-x)\tfrac{1}{2}[\bar{u}(-x) + u(-x)] \end{aligned} \quad (18)$$

and

$$\begin{aligned} H^{I=1}(x,0,0) &= \tfrac{1}{2}[H^u(x,0,0) - H^d(x,0,0)] \\ &= \tfrac{1}{2}[H^u(x,0,0) + H^u(-x,0,0)] \\ &= \theta(x)\tfrac{1}{2}[u(x) - \bar{u}(x)] \\ &\quad - \theta(-x)\tfrac{1}{2}[\bar{u}(-x) - u(-x)]. \end{aligned} \quad (19)$$

Analogous relations, with singlet $q(x) + \bar{q}(x)$ and valence, $q(x) - \bar{q}(x)$ combinations for the d quark can be easily obtained, by using Eq. (11) (see also [7]). It is worth noting that for $\xi = \Delta^+ = 0$ the ERBL region shrinks to zero and the variable x reduces to x_q [Eq. (3)]. Finally, from Eq. (16) one has a normalization for the valence combination $u_v(x) = u(x) - \bar{u}(x)$ given by $\int_0^1 dx u_v(x) = 1$.

It should be pointed out that the parton distributions represent a bridge toward the chiral-even transverse-momentum-dependent distribution (TMD) $f_1(x, |\mathbf{k}_\perp|^2)$ (see, e.g., [30–32] for the nucleon case), as shown by the following relation:

$$q(x) = \int d\mathbf{k}_\perp f_1^q(x, |\mathbf{k}_\perp|^2) \qquad (x \geq 0). \quad (20)$$

Furthermore, it is worth noting that an experimental access to $f_1(x, |\mathbf{k}_\perp|^2)$ and to other TMDs is a fundamental step in order to understand the correlations between constituents inside the pion and eventually the dynamics.

To complete this brief résumé of the general formalism, we have to mention that the sum rules in Eqs. (16) and (17) are the lowest order of the moments of the isovector and isoscalar GPDs. In particular, $H^{I=1}(x,\xi,t)$ [see Eq. (13)] has only even moments, while $H^{I=0}(x,\xi,t)$ [see Eq. (12)] has only odd moments. Moreover, it turns out (see, e.g., [4]) that the nth Mellin moments of the GPDs are polynomials of ξ with highest power n for even moments and $n+1$ for odd moments; i.e. only even powers of ξ appear, as expected from Eq. (14). It is worth noting that the so-called *polynomiality* follows from general properties, such as Hermiticity, covariance, parity, and time-reversal invariance [1,2]. The isospin-dependent moments are given by ($j \geq 0$)

$$\int_{-1}^{1} dx x^{2j} H^{I=1}(x,\xi,t) = \sum_{i=0}^{j} A^{I=1}_{2j+1,2i}(t)(2\xi)^{2i}, \quad (21)$$

$$\int_{-1}^{1} dx x^{2j+1} H^{I=0}(x,\xi,t) = \sum_{i=0}^{j+1} A^{I=0}_{2j+2,2i}(t)(2\xi)^{2i}. \quad (22)$$

In particular, numerical calculations of (i) $F_\pi(t) = A^{I=1}_{1,0}(t)$ and (ii) $A^{I=0}_{2,0} = \theta_2(t)/2$ and $A^{I=0}_{2,2} = -\theta_1(t)/8$ will be presented in Sec. VI.

In conclusion, approaches that satisfy the basic field-theoretic assumptions underlying polynomiality, i.e. extended Poincaré covariance, automatically fulfill the conditions (21) and (22). In general, such a property is an important test of consistency of the model.

III. FOCK DECOMPOSITION

Let us introduce the Fock expansion of the pion state, taking care of the colorless feature of each component and including the amplitudes inside the kets to simplify the notations in this section (see, e.g., [18,19]), viz.,

$$|\pi\rangle = |q\bar{q}\rangle + |q\bar{q};g\rangle + |q\bar{q};q\bar{q}\rangle + \cdots. \quad (23)$$

Then one can decompose the GPDs in terms of their Fock contents (see also [4,23]); i.e. one can rewrite Eqs. (4) and (5) by using, e.g.,

$$\begin{aligned} H^q(x,\xi,t) &= \sum_n^{\text{Fock}} \langle \pi;n|\Gamma^q_D|\pi;n\rangle \theta(|x| - |\xi|)\theta(1-|x|) \\ &\quad + \theta(|\xi| - |x|)\Big[\sum_n^{\text{Fock}} \langle \pi;n|\Gamma^q_{\text{ND}}|\pi;n+2\rangle\theta(\xi) \\ &\quad + \sum_n^{\text{Fock}} \langle \pi;n+2|\Gamma^q_{\text{ND}}|\pi;n\rangle\theta(-\xi)\Big] + \cdots, \end{aligned} \quad (24)$$

where n indicates the number of quarks and antiquarks, $\Gamma_{\rm D}$ and $\Gamma_{\rm ND}$ are the diagonal and nondiagonal, in the Fock space, terms of the current operator, respectively, and dots represent all of the other transition matrix elements, possibly containing states with gluons. The diagonal terms yield contributions to the valence region (DGLAP region), while the nondiagonal ones have to be considered in the nonvalence region (ERBL region). In Eq. (24), we have shown only transitions involving fermionic fields, and this explains the selection rule $\Delta n = 0, 2$.

In a simple picture of a hadron, the valence state has a dominant role at the hadron scale, and this leads one naturally to associate the DGLAP region with this Fock component.

The same decomposition can be applied to the em and gravitational form factors and to all of the t-dependent ''generalized'' form factors appearing in Eqs. (21) and (22). Clearly, this kind of decomposition could allow a deeper understanding of the dynamics related to the components beyond the valence one. As a simple application, let us consider the em form factor. From Eqs. (16) and (24), retaining only the fermionic transitions, one has

$$F_\pi^{(v)}(\xi, t) = 2\int_{|\xi|}^1 dx H^{I=1}(x, \xi, t) = 2\sum_n^{\rm Fock}\int_{|\xi|}^1 dx \langle \pi; n|\Gamma_{\rm D}^{I=1}|\pi; n\rangle, \tag{25}$$

$$F_\pi^{(nv)}(\xi, t) = 2\int_0^{|\xi|} dx H^{I=1}(x, \xi, t) = 2\sum_n^{\rm Fock}\int_0^{|\xi|} dx [\theta(\xi)\langle \pi; n|\Gamma_{\rm ND}^{I=1}|\pi; n+2\rangle + \theta(-\xi)\langle \pi; n+2|\Gamma_{\rm ND}^{I=1}|\pi; n\rangle]. \tag{26}$$

The valence term $F_\pi^{(v)}(\xi, t)$ receives the largest contribution from the valence component of the pion state, but it does not give the full result in the whole kinematical range, as indicated by the residual dependence upon ξ. The nonvalence term $F_\pi^{(nv)}(\xi, t)$ is due to contributions like the pair-production mechanism; see Fig. 2(b). The sum of Eqs. (25) and (26) leads to the full result, viz.,

$$F_\pi(t) = F_\pi^{(v)}(\xi, t) + F_\pi^{(nv)}(\xi, t), \tag{27}$$

and it is *independent of* ξ and a function of t only. One can also express the invariance of the sum under changes of ξ as

$$\frac{\partial^m}{\partial \xi^m} F_\pi^{(v)}(\xi, t) = -\frac{\partial^m}{\partial \xi^m} F_\pi^{(nv)}(\xi, t), \tag{28}$$

with $m \geq 1$. It is worth noting that all of the derivatives of $F_\pi(t)$ are independent upon ξ, and therefore relations like the one in Eq. (28) can be generalized, i.e.

$$\frac{\partial^m}{\partial \xi^m}\frac{\partial^\ell}{\partial t^\ell} F_\pi^{(v)}(\xi, t) = -\frac{\partial^m}{\partial \xi^m}\frac{\partial^\ell}{\partial t^\ell} F_\pi^{(nv)}(\xi, t), \tag{29}$$

with $m \geq 1$ and $\ell \geq 0$. As a consequence, with the help of Eq. (16), one can deduce interesting sum rules for the partial derivatives of $H^{I=1}(x, \xi, t)$.

Let us remind the reader that calculations of the elastic form factors have been performed in different frames. In particular, we have chosen (i) the Drell-Yan frame, where $\Delta^+ = 0$ and therefore $\xi = 0$ (see Ref. [18] for generalities on the Drell-Yan frame), or (ii) a Breit frame (i.e. $\Delta^+ = -\Delta^-$) where $\perp = 0$ (see [33] for an extended discussion of the motivations for adopting such a frame), and then ξ follows a kinematical trajectory in the (ξ, t) plane given by $|\xi| = 1/\sqrt{1 - 4m_\pi^2/t}$ [see below Eq. (33)]. In the first case, the em form factor is saturated by the valence contribution, because of $\xi = 0$ [cf. Eqs. (27) and (25)], while in the second frame both valence and nonvalence terms contribute, since ξ does not vanish but changes with t. For $-t^2 \gg m_\pi^2$ the value of ξ approaches 1, and therefore the nonvalence term saturates the em form factor [cf. Eqs. (27) and (26)]. In model calculations this general behavior was indeed observed [21]. It is understood that, for an experimental investigation of the whole (ξ, t) plane, different kinematical conditions are needed, also exploiting the helpful properties of the LF boosts (see, e.g., [17]).

Following the same spirit, one could extend this analysis to the other form factors that appear in Eqs. (21) and (22); i.e. one can consider the partial derivatives of the valence and nonvalence contribution to the generalized form factors $A_{2j+2,2i}^{I=0}(t)$ and $A_{2j+1,2i}^{I=1}(t)$, obtaining final relations that have the same structure as the ones in Eqs. (28) and (29).

IV. COVARIANT MODEL OF THE PION WITH PAULI-VILLARS REGULATORS

In Ref. [21], an analytic covariant model, symmetric in the exchange of the constituent four-momenta (see Refs. [34,35] for previous nonsymmetric versions), was adopted for evaluating the em form factor. In this work, a direct extension of the symmetric covariant model to DVCS is exploited for calculating the no-helicity flip GPD, in the spacelike interval $0 \geq t \geq -10$ $(\mathrm{GeV/c})^2$.

In a Breit frame, one has $\Delta^0 = 0$, i.e. $\Delta^+ = -\Delta^-$, and $\mathbf{p}' = -\mathbf{p} = \mathbf{\Delta}/2$. By choosing $\Delta^+ \geq 0$ and recalling that

$$p'^- = \frac{m_\pi^2 + |\mathbf{\Delta}_\perp|^2/4}{p'^+}, \qquad p^- = \frac{m_\pi^2 + |\mathbf{\Delta}_\perp|^2/4}{p^+},$$
$$\Delta^- = p'^- - p^- = -\Delta^+\frac{m_\pi^2 + |\mathbf{\Delta}_\perp|^2/4}{p'^+ p^+} = \Delta^-\frac{m_\pi^2 + |\mathbf{\Delta}_\perp|^2/4}{(p^+ + \Delta^+)p^+}, \tag{30}$$

one gets

$$p^+ = \frac{-\Delta^+ + \sqrt{-\Delta^2 + 4m_\pi^2}}{2} = -\frac{\Delta^+}{2}\left(1 + \frac{1}{\xi}\right),$$
$$p'^+ = \frac{\Delta^+ + \sqrt{-\Delta^2 + 4m_\pi^2}}{2} = \frac{\Delta^+}{2}\left(1 - \frac{1}{\xi}\right). \tag{31}$$

Then the following relation holds (notice that $2P^+ = \sqrt{-\Delta^2 + 4m_\pi^2}$):

$$\Delta^2 = -\Delta^{+2} - |\boldsymbol{\Delta}_\perp|^2 = -4\xi^2 P^{+2} - |\boldsymbol{\Delta}_\perp|^2$$
$$= -\xi^2(-\Delta^2 + 4m_\pi^2) - |\boldsymbol{\Delta}_\perp|^2, \tag{32}$$

which leads to a constraint on the maximal value for the variable ξ. As a matter of fact, in the spacelike region $-\Delta^2 + 4m_\pi^2 \neq 0$, and one has

$$\xi^2 = \frac{-\Delta^2 - |\boldsymbol{\Delta}_\perp|^2}{-\Delta^2 + 4m_\pi^2}. \tag{33}$$

Then the maximum value of ξ^2 is found for $\boldsymbol{\Delta}_\perp = 0$, viz.,

$$\xi^2 \leq \frac{-\Delta^2}{-\Delta^2 + 4m_\pi^2} \leq 1. \tag{34}$$

For $m_\pi = 0$ (and $\Delta^2 \neq 0$), one has

$$\xi^2 = 1 + \frac{|\boldsymbol{\Delta}_\perp|^2}{\Delta^2}. \tag{35}$$

If one additionally chooses a frame where $\boldsymbol{\Delta}_\perp = 0$ (i.e. only $\Delta_z \neq 0$), then $\xi = -1$, and therefore, in this extreme case, only the nonvalence region contributes.

A basic ingredient in the analytic covariant model of Ref. [21] is the pion BS amplitude, that can be quite well approximated by retaining only the pseudoscalar Dirac structure (see, e.g., [36]), namely,

$$\Psi(k - P, p) = -\frac{m}{f_\pi} S(k - \Delta/2)\gamma^5 \Lambda(k - P, p) S(k - P), \tag{36}$$

where $\frac{m}{f_\pi}$ is the quark-pion coupling, as suggested by a simple effective Lagrangian (see, e.g., [25]), $f_\pi = 92.4$ MeV is the pion decay constant, and m and $S(k)$ are the mass and the Dirac propagator of the CQ, respectively. In Eq. (36), $\Lambda(k - P, p)$ is a scalar function that describes the momentum-dependent part of the coupling between the constituents and the spin-0 system and plays the role of the Pauli-Villars regulator of the otherwise divergent integrals that yield GPDs or the em form factor. In particular, in this work we adopt two symmetric (in the exchange of the CQ four-momenta) covariant forms: (i) the one considered in Ref. [21], and based on the following sum:

$$\Lambda_1(k - P, p) = C_1\left\{\frac{1}{[(k - \Delta/2)^2 - m_R^2 + \imath\epsilon]} + \frac{1}{[(P - k)^2 - m_R^2 + \imath\epsilon]}\right\}, \tag{37}$$

and (ii) a natural extension based on a product, viz.,

$$\Lambda_2(k - P, p) = C_2 \frac{1}{[(k - \Delta/2)^2 - m_R^2 + \imath\epsilon]} \times \frac{1}{[(P - k)^2 - m_R^2 + \imath\epsilon]}. \tag{38}$$

This product form provides a more realistic transverse-momentum falloff, as seen from the expected behavior of the BS amplitude obtained by using a simple (one-boson-exchange) kernel (see, e.g., [37]), and this has a sizable impact on both the high-momentum tail of the em form factor and the end-point behavior of the parton distribution, as shown in the results presented in Sec. VI. We can anticipate that the most favorable comparison with the experimental data of the em form factor is obtained by using the product form, as also expected if one follows a perturbative QCD (pQCD) analysis, where a one-gluon exchange represents the leading contribution to the kernel [28,38].

In both expressions, once the constituent mass m is chosen, m_R is determined by fitting the experimental value for f_π (cf. [21]), while the constants C_1 and C_2 are fixed by exploiting the charge normalization, as discussed below.

As a final comment on the Dirac structure that appears in Eq. (36), we remind the reader that it leads to the standard Melosh rotation for a pair of fermions coupled to a total spin $S = 0$ (see [39]), once we consider the valence wave function, defined as follows (see, e.g., [19]):

$$\Phi_{\rm val}(\kappa^+, \boldsymbol{\kappa}_\perp, p) = -\frac{m}{f_\pi}\int \frac{d\kappa^-}{2\pi} S_{\rm on}(\kappa - p) \times \gamma^5 \Lambda(\kappa, p) S_{\rm on}(-\kappa), \tag{39}$$

where $S_{\rm on}(\kappa) = (\not{\kappa}_{\rm on} + m)/(\kappa^2 - m^2 + i\epsilon)$ with $\kappa^\mu_{\rm on} \equiv \{\kappa^-_{\rm on} = (m^2 + |\boldsymbol{\kappa}_\perp|^2)/\kappa^+, \kappa^+, \boldsymbol{\kappa}_\perp\}$.

The no-helicity flip GPD for the pion is calculated in the one-loop approximation (triangle diagram; cf. Fig. 1) with the BS amplitude of Eq. (36) and the symmetrical forms shown in Eqs. (37) and (38). In particular, the u-quark GPD is given in the impulse approximation by

$$H^u(x, \xi, t) = -\imath N_c \mathcal{R} \times \int \frac{d^4k}{2(2\pi)^4}\delta(P^+x - k^+) \times V^+(k, p, p')\Lambda(k - P, p')\Lambda(k - P, p), \tag{40}$$

where $N_c = 3$ is the number of colors, $\mathcal{R} = 2m^2/f_\pi^2$, and

$$V^+(k, p, p') = {\rm Tr}\left\{S(k - P)\gamma^5 S\left(k + \frac{\Delta}{2}\right)\gamma^+ S\left(k - \frac{\Delta}{2}\right)\gamma^5\right\}. \tag{41}$$

The presence of the delta function in Eq. (40), given the kinematical relations in Eq. (1), imposes the correct support $[-|\xi|, 1]$ for the variable x as discussed in detail in Appendix B (note that H^d has the support $[-1, |\xi|]$ for the variable x). A relevant feature in the analysis of the GPD,

as well as in the case of the em form factor, is given by the instantaneous term present in $S(k)$. As a matter of fact, the Dirac propagator can be decomposed using the LF kinematics as follows [18]:

$$S(k) = \frac{\not{k} + m}{k^2 - m^2 + \imath\epsilon} = S_{\rm on}(k) + \frac{\gamma^+}{2k^+} = \frac{\not{k}_{\rm on} + m}{k^+(k^- - k^-_{\rm on} + \frac{\imath\epsilon}{k^+})} + \frac{\gamma^+}{2k^+}, \tag{42}$$

where the second term, proportional to γ^+, is an instantaneous one in the LF time. It should be pointed out that the instantaneous contribution to the GPD is produced only by the spectator fermion (in the present example, an antifermion), i.e. by $S(k - P)$. Indeed, the instantaneous terms pertaining to the other propagators do not contribute, because of the property $(\gamma^+)^2 = 0$. In our symmetric model, the instantaneous term of Eq. (42) contributes to $H^u(x, \xi, t)$ both in the valence and in the nonvalence region [see Eqs. (B10)–(B15)], since we take fully into account the analytic structure of the symmetric vertex function (for a different approach, where such an analytic structure is disregarded, see [13]).

The pion em form factor is obtained by using the sum rule (16):

$$F_\pi(t) = \int_{-1}^{1} dx H^u(x, \xi, t) = -\imath N_c \frac{\mathcal{R}}{(p'^+ + p^+)} \int \frac{d^4k}{(2\pi)^4} V^+(k, p, p') \times \Lambda(k - P, p')\Lambda(k - P, p). \tag{43}$$

The last expression for $F_\pi(t)$ can be extracted directly from the Mandelstam formula for the matrix elements of the em current [20] (see, e.g., [40,41]), as well. Notice that the model preserves current conservation, as discussed in [21].

The normalization of the form factor, Eq. (43), allows us to determine C_1 and C_2 in Eqs. (37) and (38). Such a charge normalization represents the impulse approximation of the normalization condition in the fully interacting BS theory [20,42].

A standard analytic integration on k^- (see Appendix B for details) leads to the following decomposition of $H^u(x, \xi, t)$ in valence and nonvalence contributions:

$$H^u(x, \xi, t) = H^u_{(v)}(x, \xi, t)\theta(x - |\xi|)\theta(1 - x) + H^u_{(nv)}(x, \xi, t)\theta(|\xi| - x)\theta(|\xi| + x). \tag{44}$$

Notice that $H^u_{(v)}$ and $H^u_{(nv)}$ are given in Appendix B for the two momentum dependences shown in Eqs. (37) and (38).

The d-quark GPD can be obtained by recalling Eq. (9).

Within our covariant model the valence component $H^u_{(v)}$ in Eq. (44) is an approximation to the diagonal terms in Eq. (24), while the component $H^u_{(nv)}$ contains the contribution of the pair-production mechanism from an incoming virtual photon with $\Delta^+ > 0$ and approximates the nondiagonal terms.

An interesting approximation of the contribution to GPD in the valence region can be obtained once the analytic structure of the BS amplitude is disregarded and only the poles of the propagators are retained in the integration over k^- (see Appendix B). As a matter of fact [see Eq. (B7)], within the mentioned approximation

$$H^u_{(v)}(x, \xi, t) \sim H^u_{(v)\rm on}(x, \xi, t) = -\frac{N_c \mathcal{R}}{4(2\pi)^3} \int d\boldsymbol{\kappa}_\perp \int_0^{p^+} d\kappa^+ \times \frac{\delta[P^+(1 - x) - \kappa^+]}{\kappa^+(p^+ - \kappa^+)(p'^+ - \kappa^+)} \mathrm{Tr}[\mathcal{O}^+(\kappa^-_{\rm on})] \times \frac{\Lambda(\kappa, p)|_{\kappa^-_{\rm on}}}{[p^- - \kappa^-_{\rm on} - (p - \kappa)^-_{\rm on}]} \times \frac{\Lambda(\kappa, p')|_{\kappa^-_{\rm on}}}{[p'^- - \kappa^-_{\rm on} - (p' - \kappa)^-_{\rm on}]}, \tag{45}$$

where $\kappa = P - k$, $\kappa^-_{\rm on} = (m^2 + |\boldsymbol{\kappa}_\perp|^2)/\kappa^+$, and

$$\mathrm{Tr}[\mathcal{O}^+(\kappa^-_{\rm on})] = \mathrm{Tr}\{(\not{\kappa}_{\rm on} + m)[(\not{p}' - \not{\kappa})_{\rm on} + m] \times \gamma^+[(\not{p} - \not{\kappa})_{\rm on} + m]\}. \tag{46}$$

Moreover, if in Eq. (45) we identify the following ratio:

$$\frac{\Lambda(\kappa, p)|_{\kappa_{\rm on}}}{[p^- - \kappa^-_{\rm on} - (p - \kappa)^-_{\rm on}]}$$

with a model LF wave function, then the final expression coincides with the result obtained within a LFHD approach (see the following Sec. V B), since the trace $\mathrm{Tr}[\mathcal{O}^+(\kappa^-_{\rm on})]$ generates the correct Melosh-rotation factor [39]. We would stress that the identification is meaningful once the analytic structure of the BS amplitude is disregarded.

V. LIGHT-FRONT MODELS OF THE PION

In this section we present models that at different extent (i) fulfill the Poincaré covariance and (ii) take into account the Fock components of the pion state beyond the valence contribution. A first important difference between the models is given by the frame we choose. In the approach we call the Mandelstam-inspired LF model, a Breit frame, where $\boldsymbol{\Delta}_\perp = 0$, is considered. This choice was followed in Ref. [22] in order to perform a microscopical calculation of the em pion form factor in both the space- and timelike regions. It should be pointed out that such a frame leads one to consider contributions from a pair-production mechanism, differently from what happens in a Drell-Yan frame, where $\Delta^+ = 0$. This second frame is the one adopted in the second approach illustrated in this section, based on a LF Hamiltonian dynamics description of the pion state (see, e.g., [17] for a general review of LFHD).

A. Mandelstam-inspired LF model

In Ref. [22] an approach was elaborated to calculate the em form factor of the pion starting from a covariant expression of the matrix elements of the current given by the Mandelstam formula [20] [cf. also Eq. (40)]. Moreover, a microscopic VMD was used for dressing the quark-photon vertex. The dynamical inputs of such an approach were the wave functions of both the pion and vector mesons, taken as eigenstates of the relativistic CQ square mass operator of Ref. [43], which includes both confinement, through a harmonic oscillator potential, and $\pi-\rho$ splitting through a Dirac-delta interaction in the pseudoscalar channel. In what follows we apply the same approach for evaluating the no-helicity flip GPDs.

Let us first illustrate the kinematics in the adopted frame, where $\boldsymbol{\Delta}_\perp = 0$ (i.e. $\Delta^- = \Delta^2/\Delta^+$) and $\boldsymbol{p}_\perp = \boldsymbol{p}'_\perp = 0$. Then in the spacelike region, for $\Delta^+ \geq 0$, one has for p^+ and p'^+

$$\begin{aligned} p^+ &= \frac{\Delta^+}{2}\left(-1+\sqrt{1-4\frac{m_\pi^2}{\Delta^2}}\right) = -\frac{\Delta^+}{2}\left(1+\frac{1}{\xi}\right), \\ p'^+ &= \frac{\Delta^+}{2}\left(1+\sqrt{1-4\frac{m_\pi^2}{\Delta^2}}\right) = \frac{\Delta^+}{2}\left(1-\frac{1}{\xi}\right), \end{aligned} \tag{47}$$

since

$$\begin{aligned} p'^- &= \frac{m_\pi^2}{p'^+}, \qquad p^- = \frac{m_\pi^2}{p^+}, \\ \Delta^- &= p'^- - p^- = -\Delta^+ \frac{m_\pi^2}{(p^+ + \Delta^+)p^+}. \end{aligned} \tag{48}$$

The following simple relation between ξ and Δ^2 holds:

$$\xi = -\frac{\Delta^+}{2P^+} = -\frac{\Delta^+}{(p'^+ + p^+)} = -\frac{1}{\sqrt{1-4\frac{m_\pi^2}{\Delta^2}}}. \tag{49}$$

It is easily seen that, if $m_\pi = 0$, one has $\xi = -1$ for any Δ^2.

Extending the approach of Ref. [22], one can find for the quark GPD the same formal expression of Eq. (40), but (i) a microscopic VMD dressing $\Gamma^\mu(k,\Delta)$ is considered instead of the bare quark-photon vertex γ^μ, and (ii) phenomenological *Ansätze* for the BS amplitudes in the valence and nonvalence regions are adopted. Another basic difference with respect to the analytic model presented in the previous section is that only the simple analytic structure of the Dirac propagators is retained; i.e. the analytic structure is disregarded in the BS amplitudes of both (i) the initial and final pions and (ii) the VM dressing of the quark-photon vertex. This approximation turns out to be a very effective one in the calculation of the em form factor just in the $\boldsymbol{\Delta}_\perp = 0$ frame [44].

In Ref. [22], a further simplification in the calculation was achieved by a quite natural assumption, namely, a vanishing pion mass. Within such an approximation, only diagrams with a $q\bar{q}$ production contribute [cf. Fig. 2(b)], and this implies the necessity to introduce the VMD dressing. We have to stress that a bare term is missing, due to the vanishing pion mass (cf. the discussion in [22]). Therefore, in the quark-photon vertex for the covariant model, Eq. (41), the Dirac matrix γ^+ is replaced by the plus component of the following four-vector that microscopically describes a VM dressing. For $t \leq 0$ one has

$$\Gamma^\mu(k,\Delta) = \sqrt{2}\sum_{n,\lambda}[\boldsymbol{\epsilon}_\lambda \cdot \hat{V}_n(k,P_n)]\Lambda_n(k,P_n)\frac{[\epsilon_\lambda^\mu]^* f_{Vn}}{(t-M_n^2)}, \tag{50}$$

where f_{Vn} is the decay constant of the nth VM into a virtual photon (*calculated in the model*), $P_n^\mu \equiv \{M_n^2/\Delta^+, \Delta^+, \mathbf{0}_\perp\}$ is the four-momentum of an on-mass-shell VM with a square mass given by $P_n^2 = M_n^2$, and $\boldsymbol{\epsilon}_\lambda(P_n)$ is its polarization. Moreover, the VM BS amplitude is approximated as follows:

$$\begin{aligned} \Psi_{n\lambda}(k,P_n) = \frac{\not{k}+m}{k^2-m^2+\imath\epsilon}[\boldsymbol{\epsilon}_\lambda(P_n)\cdot\hat{V}_n(k,P_n)]\Lambda_n(k,P_n) \\ \times \frac{\not{k}-\not{P}_n+m}{(k-P_n)^2-m^2+\imath\epsilon}, \end{aligned} \tag{51}$$

where $\hat{V}_n(k,P_n)$ is the proper Dirac structure and $\Lambda_n(k,P_n)$ the momentum-dependent part, approximated on the LF hyperplane, as discussed below.

In the valence sector, after performing the k^- integration, both pion and VM BS amplitudes reduce to 3D amplitudes with one constituent on its mass shell. In Ref. [22], the momentum-dependent part of the on-shell VM BS amplitude (that contains on both sides proper Dirac projectors) is described through a LF VM wave function, i.e.

$$\frac{P_n^+\Lambda_n(k,P_n)|_{k^-=k^-_{\rm on}}}{[M_n^2 - M_0^2(k^+,\mathbf{k}_\perp;P_n^+)]} = \psi_n(k^+,\mathbf{k}_\perp;P_n^+) \tag{52}$$

and

$$M_0^2(k^+,\mathbf{k}_\perp;P_n^+)] = P_n^+[k^-_{\rm on} + (P_n-k)^-_{\rm on}].$$

In Eq. (52), $\psi_n(k^+,\mathbf{k}_\perp;P_n^+)$ is an eigenfunction of the relativistic CQ square mass operator of Ref. [43], as mentioned at the beginning of this section. Moreover, it is normalized to the probability of the valence Fock state, according to the model elaborated in Ref. [22].

The valence component of the pion was modeled adopting an analogous ansatz. Moreover, in Ref. [22] two different calculations were generated by using (i) the pion eigenstate of the model in Ref. [43] and ii) the pQCD asymptotic wave function (see, e.g., [28]).

In the nonvalence region, namely, the only region contributing to the GPDs for $m_\pi = 0$ [see Eq. (49)], besides the pion valence component in the initial state one has to deal with a nonvalence component of the pion state, since the process depicted in Fig. 2(b) can be interpreted as a

transition from a state composed by the valence component of the initial pion and the virtual photon, $|q\bar{q}, \gamma^*\rangle$, to a higher Fock component, $|q\bar{q}, q\bar{q}\rangle$, pertaining to the final pion. At the level of the pion BS amplitudes, one has to model an off-shell BS amplitude that takes into account the absorption of the initial pion by an antiquark [according to the case illustrated in Fig. 2(b)]. In Ref. [22], a simple ansatz, namely, a constant vertex, was assumed, like in Ref. [45]. Notice that such a coupling constant is fixed by the normalization of the pion form factor, since the diagram shown in Fig. 2(a) does not contribute, as a consequence of the simplification $m_\pi = 0$.

Within the approach presented in this subsection, since $|\xi| = 1$ (given the vanishing m_π), the quark GPD has only a contribution from $H^u_{(\mathrm{nv})}$, i.e.

$$H^u(x, |\xi| = 1, t) = H^u_{(nv)}(x, |\xi| = 1, t)\theta(1 - x)\theta(1 + x), \tag{53}$$

where, by introducing $\kappa = P - k$,

$$H^u_{(nv)}(x, |\xi| = 1, t) = -\sum_n \frac{f_{Vn}}{t - M_n^2} \frac{N_c}{(2\pi)^3} \frac{\mathcal{D}_\pi}{\sqrt{2}} \int_{p^+}^{p'^+} \frac{d\kappa^+ \delta[P^+(1 - x) - \kappa^+]}{\kappa^+(p'^+ - \kappa^+)(p^+ - \kappa^+)} \times \int d\boldsymbol{\kappa}_\perp \left\{ \frac{\psi_n((p' - \kappa)^+, -\boldsymbol{\kappa}_\perp; P_n^+)[M_n^2 - M_0^2(\kappa^+, \boldsymbol{\kappa}_\perp; P_n^+)]}{[t - M_0^2(\kappa^+, \boldsymbol{\kappa}_\perp; P_n^+) + i\epsilon]} \mathcal{I}_1 + \psi^*_\pi((p' - \kappa)^+, -\boldsymbol{\kappa}_\perp; p'^+)\mathcal{I}_2 \right\}, \tag{54}$$

where $\mathcal{D}_\pi$ is the constant describing the off-shell quark-pion vertex, while $\mathcal{I}_1$ and $\mathcal{I}_2$ are given by

$$\begin{aligned}
\mathcal{I}_1 &= -\frac{1}{2}\frac{m}{f_\pi}\Lambda((p' - \kappa), p')|_{\kappa^- = p'^- - (p' - \kappa)^-_{\mathrm{on}}} \\
&\quad \times \mathrm{Tr}\{\gamma^+[(\not{p}' - \not{\kappa})_{\mathrm{on}} + m] \\
&\quad \times [\hat{V}_{\mathrm{nz}}(p' - \kappa, P_n)]_{\mathrm{on}}[(\not{p} - \not{\kappa})_{\mathrm{on}} + m]\}, \\
\mathcal{I}_2 &= \frac{1}{2}\mathrm{Tr}\{(\not{\kappa}_{\mathrm{on}} + m)[(\not{p}' - \not{\kappa})_{\mathrm{on}} + m] \\
&\quad \times [\hat{V}_{\mathrm{nz}}(p' - \kappa, P_n)]_{\mathrm{on}}\gamma^+\} \\
&\quad \times \Lambda_n(p' - \kappa, P_n)|_{\kappa^- = p'^- - (p' - \kappa)^-_{\mathrm{on}}}.
\end{aligned} \tag{55}$$

The Dirac structure $[\hat{V}^\mu_n(p' - \kappa, P_n)]_{\mathrm{on}}$, where all of the constituents are on their own mass shell, is chosen in order to generate the proper Melosh rotations for $^3S_1$ states [39]. Furthermore, the traces previously shown contain the instantaneous terms [see Eq. (42)] that survive after assuming $m_\pi = 0$. In order to model the instantaneous part of the vertex functions directly attached to γ^+, we performed the following replacements:

$$\begin{aligned}
&\frac{m}{f_\pi}\Lambda((p' - \kappa), p')|_{\kappa^- = p'^- - (p' - \kappa)^-_{\mathrm{on}}} \\
&\quad \to \mathcal{C}_\pi \psi_\pi(\kappa^+, \boldsymbol{\kappa}_\perp; p'^+)\frac{[m_\pi^2 - M_0^2(\kappa^+, \boldsymbol{\kappa}_\perp; p'^+)]}{p'^+}
\end{aligned} \tag{56}$$

for the pion and

$$\begin{aligned}
&\Lambda_n((p' - \kappa), P_n)|_{\kappa^- = p'^- - (p' - \kappa)^-_{\mathrm{on}}} \\
&\quad \to \mathcal{C}_{\mathrm{VM}}\psi_n((p' - \kappa)^+, -\boldsymbol{\kappa}_\perp; P_n^+) \\
&\qquad \times \frac{[M_n^2 - M_0^2((p' - \kappa)^+, -\boldsymbol{\kappa}_\perp; P_n^+)]}{P_n^+}
\end{aligned} \tag{57}$$

for the VMs, as in Ref. [22]. In Eqs. (56) and (57), the constants $\mathcal{C}_\pi$ and $\mathcal{C}_{\mathrm{VM}}$ roughly describe the effects of the short-range interaction. Indeed, a relative weight $w_{\mathrm{VM}} = \mathcal{C}_{\mathrm{VM}}/\mathcal{C}_\pi$ can be used as a free parameter. Let us remind the reader that the on-shell parts of the BS amplitudes have on the left and right sides the proper Dirac projectors.

Finally, it is worth noting that the results presented in the following Sec. VI have been calculated by using all of the parameters adopted in Ref. [22], but with a CQ mass $m = 200$ MeV and $w_{\mathrm{VM}} = -1$ (see [22] for $m = 265$ MeV and different values for w_{VM}). It should be pointed out that only one adjusted parameter is necessary for describing the em form factor in the spacelike region.

The model remains invariant for kinematical transformation, after the approximation we have applied.

B. Light-front Hamiltonian dynamics model

Within a LFHD approach (see [17] for a review of the three forms of the relativistic HD introduced by Dirac in [46]), the Poincaré covariance of the description of the pion can be fully implemented, once the current operator is chosen in order to fulfill the proper commutation rules with respect to all of the generators (i.e. both the kinematical and the dynamical ones). A widely adopted strategy, within the LFHD approach, is to model the em current by using a one-body operator, but in the Drell-Yan frame, i.e. where $\Delta^+ = 0$. For instance, in this frame the em form factor can be obtained by using only the matrix elements of the plus component of the current operator, and this allows one to overcome some difficulties that manifestly appear for hadrons with angular momentum ≥ 1 (see [17,33] for a general discussion).

In the Drell-Yan frame, $\boldsymbol{\Delta}_\perp \neq 0$ and one can choose $\boldsymbol{p}'_\perp = -\boldsymbol{p}_\perp = \boldsymbol{\Delta}_\perp/2$. It is worth noting that only the spacelike region can be addressed, since $\Delta^2 = -|\boldsymbol{\Delta}_\perp|^2$. Moreover, one has $p^+ = p'^+$ and therefore $\xi = 0$ for any Δ^2.

In this section, the LFHD model with CQs, already successfully applied for describing the charge form factor and decay constant of the pion [47,48], is adopted for investigating the DGLAP contribution to the no-helicity flip GPD. This corresponds to considering in the Fock-space expansion of Eq. (24) the diagonal contribution with $n = 2$ constituents [i.e. the valence component; cf. also Eq. (39), introducing the explicit representation in terms of overlap of light-cone wave functions (LCWFs) [18,23]]. The quark contribution to the GPD in the region $0 \le x \le 1$ can be written in terms of the LCWF $\Psi_\pi(x, \boldsymbol{\kappa}_\perp; \lambda_q, \lambda_{\bar{q}})$ for the quark-antiquark system as

$$\begin{aligned} H^u(x, \xi = 0, t) = & \sum_{\lambda_q', \lambda_q, \lambda_{\bar{q}}} \int \frac{d\mathbf{k}_\perp}{2(2\pi)^3} \Psi_\pi^*(x, \boldsymbol{\kappa}_\perp'; \lambda_q', \lambda_{\bar{q}}) \\ & \times \frac{\bar{u}(x, \mathbf{k}_\perp + \frac{\boldsymbol{\Delta}_\perp}{2}, \lambda_q')}{\sqrt{k^+ + \frac{\Delta^+}{2}}} \gamma^+ \\ & \times \frac{u(x, \mathbf{k}_\perp - \frac{\boldsymbol{\Delta}_\perp}{2}, \lambda_q)}{\sqrt{k^+ - \frac{\Delta^+}{2}}} \Psi_\pi(x, \boldsymbol{\kappa}_\perp; \lambda_q, \lambda_{\bar{q}}) \\ = & \sum_{\lambda_q, \lambda_{\bar{q}}} \int \frac{d\boldsymbol{\kappa}_\perp}{2(2\pi)^3} \Psi_\pi^*(x, \boldsymbol{\kappa}_\perp'; \lambda_q, \lambda_{\bar{q}}) \\ & \times \Psi_\pi(x, \boldsymbol{\kappa}_\perp; \lambda_q, \lambda_{\bar{q}}), \end{aligned} \tag{58}$$

where $u(x, \boldsymbol{\kappa}_\perp, \lambda)$ is a LF Dirac spinor (see, e.g., [39]) and λ_i are the spin projections. The perpendicular component of the active quark momenta, $\mathbf{k}_\perp \pm_\perp /2$, becomes in the intrinsic frame

$$\begin{aligned} \boldsymbol{\kappa}_\perp &= \mathbf{k}_\perp - (1-x)\frac{\boldsymbol{\Delta}_\perp}{2}, \\ \boldsymbol{\kappa}_\perp' &= \mathbf{k}_\perp + (1-x)\frac{\boldsymbol{\Delta}_\perp}{2} = \boldsymbol{\kappa}_\perp + (1-x)\boldsymbol{\Delta}_\perp, \end{aligned} \tag{59}$$

with x given by Eq. (1). Notice that in the Drell-Yan frame $x_q = x$ [cf. Eq. (3)], since $\xi = 0$.

For the model calculation, we use a phenomenological LCWF which satisfies Poincaré covariance and is an eigenstate of the total angular momentum operator in the light-front dynamics. As outlined in Ref. [47], these properties can be fulfilled by constructing the wave function as the product of a momentum wave function $\psi(x, \boldsymbol{\kappa}_\perp)$, which is spherically symmetric and invariant under permutations, and a spin wave function, which is uniquely determined by symmetry requirements. Therefore, within LFHD one has

$$\begin{aligned} \Psi_\pi(x, \boldsymbol{\kappa}_\perp; \lambda_q, \lambda_{\bar{q}}) = & \psi_\pi(x, \boldsymbol{\kappa}_\perp) \sum_{\mu_q, \mu_{\bar{q}}} \left(\frac{1}{2}\mu_q \frac{1}{2}\mu_{\bar{q}} | 00\right) \\ & \times D^{1/2*}_{\mu_q \lambda_q}[R_M(\boldsymbol{\kappa})] D^{1/2*}_{\mu_{\bar{q}} \lambda_{\bar{q}}}[R_M(-\boldsymbol{\kappa})], \end{aligned} \tag{60}$$

where $\boldsymbol{\kappa} \equiv \{\boldsymbol{\kappa}_\perp, \kappa_z\}$ with

$$\kappa_z = M_0(x, \boldsymbol{\kappa}_\perp)(x - \tfrac{1}{2}), \tag{61}$$

and the free mass defined by

$$M_0^2(x, \boldsymbol{\kappa}_\perp) = \frac{m^2 + |\boldsymbol{\kappa}_\perp|^2}{x(1-x)}. \tag{62}$$

The spin-dependent part contains the Melosh rotations $R_M(\boldsymbol{\kappa})$ which convert the instant-form spins of both the quark and antiquark into LF spins and ensure the rotational invariance of the pion wave function. The representation of the Melosh rotation is explicitly given by

$$\begin{aligned} D^{1/2}_{\lambda\mu}[R_M(\boldsymbol{\kappa})] &= \langle \lambda | R_M(\boldsymbol{\kappa}) | \mu \rangle \\ &= \langle \lambda | \frac{m + xM_0(x, \boldsymbol{\kappa}_\perp) - i\boldsymbol{\sigma} \cdot (\hat{\mathbf{z}} \times \boldsymbol{\kappa}_\perp)}{\sqrt{(m + xM_0(x, \boldsymbol{\kappa}_\perp))^2 + \boldsymbol{\kappa}_\perp^2}} | \mu \rangle. \end{aligned} \tag{63}$$

For the momentum-dependent part of the pion wave function, we adopt the following exponential form used in Refs. [47,48]:

$$\begin{aligned} \psi_\pi(x, \boldsymbol{\kappa}_\perp) = & [2(2\pi)^3]^{1/2} \left(\frac{M_0(x, \boldsymbol{\kappa}_\perp)}{4x(1-x)}\right)^{1/2} \frac{1}{\pi^{3/4}\beta^{3/2}} \\ & \times \exp(-\kappa^2/(2\beta^2)). \end{aligned} \tag{64}$$

The wave function in Eq. (64) is normalized as

$$\int_0^1 dx \int \frac{d\boldsymbol{\kappa}_\perp}{2(2\pi)^3} |\psi_\pi(x, \boldsymbol{\kappa}_\perp)|^2 = 1$$

[recalling that $d\kappa_z = dx M_0(x, \boldsymbol{\kappa}_\perp)/[4x(1-x)]]$ and depends on the free parameter β and the quark mass m, which have been fitted to the pion charge radius and decay constant.

Inserting the model wave function of Eq. (60) in the LCWF overlap representation of GPD in Eq. (58), one obtains

$$\begin{aligned} H^u(x, \xi = 0, t) = & \int \frac{d\boldsymbol{\kappa}_\perp}{2(2\pi)^3} \psi_\pi(x, \boldsymbol{\kappa}_\perp') \psi_\pi(x, \boldsymbol{\kappa}_\perp) \\ & \times \frac{m^2 + \boldsymbol{\kappa}_\perp' \cdot \boldsymbol{\kappa}_\perp}{x(1-x) M_0(x, \boldsymbol{\kappa}_\perp') M_0(x, \boldsymbol{\kappa}_\perp)}. \end{aligned} \tag{65}$$

In the forward limit $\Delta^\mu \to 0$, the Melosh-rotation matrices combine to the identity matrix, and one obtains the ordinary parton distribution as the momentum density distribution given by the square of the momentum-dependent part of the wave function [18]; i.e. for $x \ge 0$ one gets

$$u(x) = \int \frac{d\boldsymbol{\kappa}_\perp}{2(2\pi)^3} |\psi(x, \boldsymbol{\kappa}_\perp)|^2. \tag{66}$$

VI. RESULTS AND DISCUSSION

In this section the results obtained from the different models described in the previous sections are presented and discussed. Let us first illustrate the actual values of the parameters entering the three models.

For the covariant model (Sec. IV), the CQ mass and the pion mass have values $m = 220$ MeV and $m_\pi = 140$ MeV, respectively. It should be pointed out that, for some runs, the value $m_\pi = 0$ has been used in order to match the vanishing pion mass adopted for the Mandelstam-inspired model (see Sec. V A). This change will be adequately emphasized whenever applied (in this case, the CQ mass is a little bit lowered, i.e. $m = 210$ MeV). The parameter m_R present in the pion Bethe-Salpeter amplitudes is fixed through the pion decay constant, obtaining $m_R = 600$ MeV for the sum form [Eq. (37)] and $m_R = 1200$ MeV for the product form [Eq. (38)].

In the Mandelstam-inspired model, as already mentioned, all of the parameters are the same ones used in Ref. [22], except for (i) $w_{\rm VM} = -1$ that yields the relative weight of the instantaneous contributions and (ii) the CQ mass $m = 200$ MeV, i.e. the one adopted in Ref. [49] within the same approach for the very detailed description of the nucleon em form factors in both the spacelike and the timelike region. As already mentioned, given the complexity of the calculation, a simplifying assumption of a vanishing pion mass has been also added. Finally, in the VM dressing of the quark-photon vertex [cf. Eq. (50)] up to 20 isovector mesons have been considered in order to have a good convergence even for $t = -10$ $(\mathrm{GeV}/c)^2$.

In the LFHD model (see Sec. V B), a CQ mass $m = 250$ MeV and a wave-function parameter $\beta = 319.4$ MeV have been used in order to reproduce the pion charge radius ($r_{\rm ch} = 0.670 \pm 0.02$ fm) and the pion decay constant [48].

First of all, the theoretical models have been compared with available experimental data, in particular, the pion em form factor in the spacelike region.

Figure 3 shows the ratio between the spacelike form factors, calculated by using our models, and the monopole form factor $F_{\rm mon} = 1/(1 + |t|/m_\rho^2)$ ($m_\rho = 0.770$ GeV). The relevance of such a presentation of the form factor is twofold: (i) Dividing by $F_{\rm mon}$ allows one to avoid the log plot that hinders a detailed analysis; (ii) more importantly, one can immediately discriminate between models that produce a divergent charge density at short distances and models that do not (cf. e.g., [50]), since their falloff is more rapid than $F_{\rm mon}$.

For the sake of completeness, we have also displayed two different fits (thick solid and dotted-dashed lines in Fig. 3) to the lattice data as obtained in Ref. [51]. In that paper, lattice data have been extrapolated to the experimental pion mass, and they were described up to $t = -4$ $(\mathrm{GeV}/c)^2$ in terms of both (i) a monopole function $F_\pi^{\rm lat}(t) = 1/[1 - t/M^2(m_\pi^{\rm phys})]$, with $M(m_\pi^{\rm phys}) = 0.727$ GeV, and (ii) a function with a falloff faster than the monopole one, i.e. $F_\pi^{\rm lat}(t) = 1/[1 - t/(pM^2(m_\pi^{\rm phys})]^p$, with $p = 1.173 \pm 0.058$ and $M(m_\pi^{\rm phys}) = 0.757 \pm 0.018$ GeV. In Fig. 3, the lattice results have been arbitrarily extended by using the previous functions from $t = -4$ $(\mathrm{GeV}/c)^2$ to $t = -10$ $(\mathrm{GeV}/c)^2$, with a quite reasonable outcome.

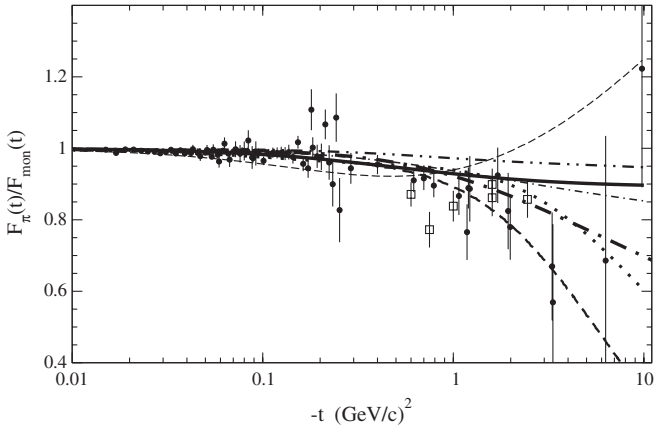

FIG. 3. Pion form factor vs $-t$. Thin dashed line: Covariant symmetric model of Ref. [21], with the momentum dependence of the pion Bethe-Salpeter amplitude given by the sum form of Eq. (37), and $m_\pi = 140$ MeV. Double-dotted-dashed line: Calculation performed within the LF Mandelstam-inspired model (cf. Sec. V A), by using an asymptotic pion wave function [28] with $m_\pi = 0$ and adopting a CQ mass of $m = 200$ MeV (notice that in Ref. [22] $m = 265$ MeV). Thick solid line: Monopole fit to lattice data as obtained in Ref. [51], arbitrarily extended in this figure from -4 to -10 $(\mathrm{GeV}/c)^2$ (see text). Thick dotted-dashed line: Faster-than-monopole fit to lattice data as obtained in Ref. [51], arbitrarily extended in this figure from -4 to -10 $(\mathrm{GeV}/c)^2$ (see text). Dotted-dashed line: The same as the double-dotted-dashed line but with a nonperturbative pion wave function, eigenstate of the squared LF mass operator of Ref. [43]. Dotted line: The same as the thin dashed line but with the product form of Eq. (38) for the pion Bethe-Salpeter amplitude. Thick dashed line: LFHD model (cf. Sec. V B) with a Gaussian pion wave function and the proper Melosh rotations. Experimental data: Full dots from the collection of Ref. [52]; open squares: Thomas Jefferson Lab data from Ref. [53].

To show the sensitivity of the covariant model of Sec. IV upon the change of the pion mass, a comparison between calculations performed with a vanishing pion mass and with $m_\pi = 140$ MeV is presented in Fig. 4. These calculations are helpful in view of the following comparisons with the Mandelstam-inspired model, where the value $m_\pi = 0$ has been adopted. It is interesting to notice from Figs. 3 and 4 that the sum form for the BS amplitude is unable to accurately describe the experimental em form factor at high values of $|t|$.

In order to illustrate the frame dependence of the Fock decomposition of the em form factor, in Fig. 5 the valence and nonvalence contributions to the pion form factor [Eq. (27)] within the covariant model based on the product

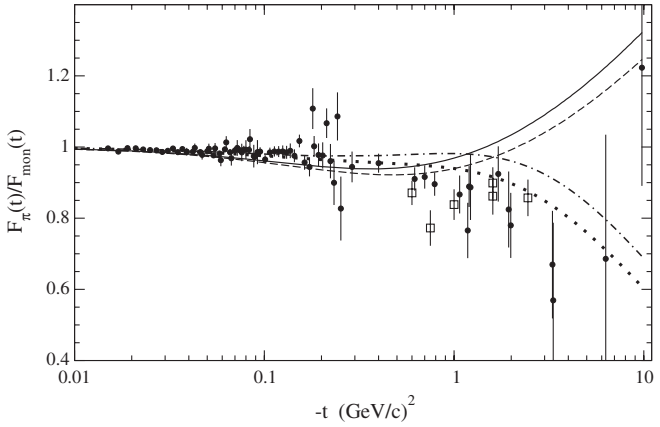

FIG. 4. Pion form factor calculated within the covariant model of Sec. IV, with and without a vanishing pion mass. Solid line: Sum form for the pion Bethe-Salpeter amplitude [Eq. (37)] and $m_\pi = 0$. Dashed line: The same as the solid line, but with $m_\pi = 140$ MeV. Dotted-dashed line: Product form for the pion Bethe-Salpeter amplitude [Eq. (38)] and $m_\pi = 0$. Dotted line: The same as the dashed-dotted line, but with $m_\pi = 140$ MeV. Experimental data as in Fig. 3.

form and $m_\pi = 0$ are presented. Such a choice for m_π is suggested [cf. Eq. (35)] by the need to explore the whole range $0 \leq |\xi| \leq 1$. The sum of the two contributions becomes ξ independent, and the result is shown in Fig. 4 by the dotted-dashed line. Figure 5 allows us to disentangle the valence and nonvalence contributions. Indeed, different values of ξ correspond to different choices of the frame (let us remind the reader that $\xi = 0$ corresponds to the Drell-Yan frame and $\xi = -1$ to the frame where $\mathbf{\Delta}_\perp = 0$). Moreover, it is worth noting that the operator "number of constituents" does not commute with the whole set of the Poincaré generators, and therefore a change of frame alters the nonvalence content. The knowledge of valence and nonvalence contributions in the plane (ξ, t) could impose new constraints to models that aim to go beyond the standard CQM.

After completing the analysis of the em form factor within our models, in Fig. 6, the isovector GPD for positive x, namely, $H^{I=1}(x, 0, 0) = u_v(x)/2$ [see Eq. (19)], is shown as a function of $x \equiv x_q$ [since for $\xi = 0$ one recovers the longitudinal-momentum fraction, Eq. (3)]. It should be pointed out that, at this stage of our analysis, no evolution has been applied. The effects of the evolution for the parton distribution will be considered elsewhere, together with a study of the evolution for the whole GPD. Calculations for the covariant model of Sec. IV and the LFHD model of Sec. V B are shown in Fig. 6. Notice that the Mandelstam-inspired LF model presently allows predictions only for $|\xi| = 1$. In order to extend to $\xi = 0$ this approach, a nonvanishing value of m_π and a bare term, besides the VMD one, should be considered. Thus one can take into account the contribution depicted in Fig. 2(a) that produces the valence term in $H^{I=1}(x, \xi, t)$, but new, nontrivial parameters have to be added (cf. the nucleon case in [49]).

The comparison in Fig. 6 shows the difficulty of the sum form [Eq. (37)] for the pion Bethe-Salpeter amplitude to give a realistic parton distribution, i.e. to have a vanishing value at the end points. Recalling that, for $\xi = 0$, the presence of the delta function in Eq. (40) and the kinematical relations in Eq. (1) impose the correct support $[0, 1]$ for the variable x (recall that, for $\xi = 0$, one has $x = x_q$), the

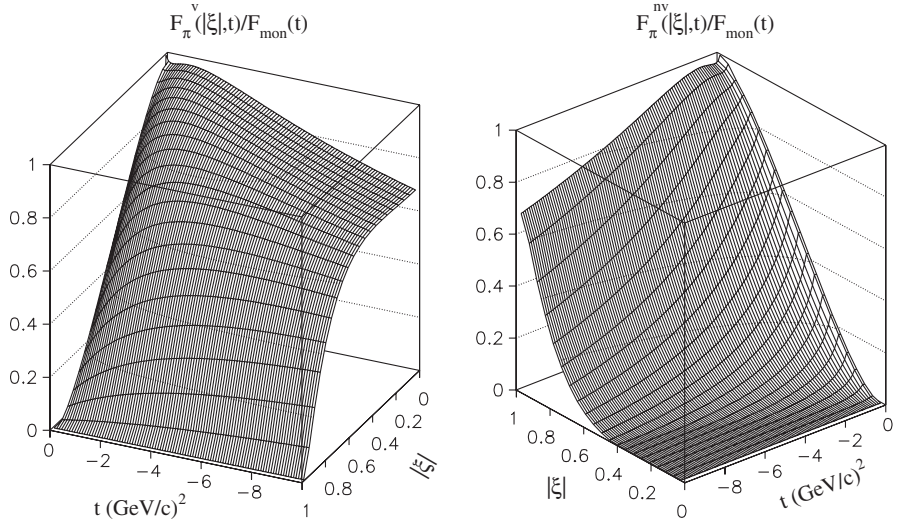

FIG. 5. Left panel: Valence contribution $F_\pi^{(v)}(|\xi|, t)$ to the em pion form factor [see Eq. (25)], evaluated within the covariant symmetric model of Sec. IV by using the product form for the momentum-dependent part of the Bethe-Salpeter amplitude [cf. Eq. (38)] and choosing $m_\pi = 0$ for covering the whole range $0 \leq |\xi| \leq 1$, according to Eq. (35). Right panel: The same as in the left panel, but for the nonvalence contribution $F_\pi^{(nv)}(|\xi|, t)$ [see Eq. (26)]. Note the different orientations of the axes in the two panels, for a straightforward selection of the relevant regions.

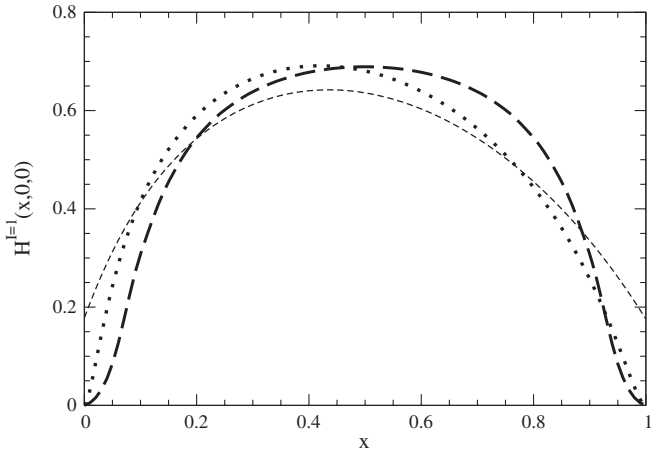

FIG. 6. Isovector GPD $H^{I=1}(x, 0, 0)$, equal to half of the parton distribution [see Eq. (19)], vs x. Thin dashed line: Covariant model of Sec. IV, calculated by using the sum form [Eq. (37)] for the pion Bethe-Salpeter amplitude and $m_\pi = 140$ MeV. Dotted line: The same as the thin dashed line, but for the product form [Eq. (38)]. Thick dashed line: LFHD model of Sec. V B, with a Gaussian pion wave function and the proper Melosh rotations. The variable x, given in Eq. (1), coincides with the usual LF longitudinal fraction x_q, since $\xi = 0$ [see text below Eq. (10)].

sum form produces a discontinuity at the end points, i.e. an infinite derivative. It is instructive to correlate such a drawback to the one already seen in Fig. 3, where the sum form is not able to reproduce the em form factor at high values of $(-t)$. Indeed, in both cases, the high-momentum part of the valence component of the pion state is involved. As a matter of fact, for $x = 0$ and $x = 1$, the intrinsic three-momentum becomes infinite [cf. Eqs. (61) and (62)], and therefore small distances are involved, just as in the case of the tail of the em form factor, where the influence upon the small-r part of the pion wave function is felt. The more realistic behavior of the product form (38) can be ascribed to a $|\mathbf{k}_\perp|$ falloff like the one dictated by a BS kernel dominated by a one-gluon exchange, as already pointed out in Sec. IV. An important, final remark is the clear shift towards small x of the curves evaluated within the covariant model, while the prediction obtained within the LFHD model is symmetric with respect to $x = 1/2$. Such an interesting difference could be explained by the fact that the full covariance of the model of Sec. IV together with its dynamical content, related to the adjusted parameter m_R, could take into account some effects beyond the pure $q\bar{q}$ component of the pion state. First, one should note that the valence component [Eq. (39)] generates a quark distribution symmetric with respect to $x = 1/2$ and a probability definitely less than 1: For the sum form $P_{\rm val} = 0.78$, and for the product form $P_{\rm val} = 0.84$ (see also [21]). Then, by using the Fock decomposition of the pion state (see, e.g., [4] for a general discussion), one immediately recognizes contributions from both the $q\bar{q}$ component (i.e. the valence component) and from other components with more constituents [see, e.g., the instantaneous contributions in Eqs. (B10)–(B12) and the analysis in [54]]. Thus, the active quark shares the longitudinal momentum of the pion with more than one spectator parton, belonging to the Fock-space configuration beyond the valence one. Therefore, the shift toward values of x less than $1/2$ is expected, since our covariant model contains more physical effects than the basic one. In particular, for a nonvanishing pion mass the average longitudinal-momentum fraction for the sum form is $\langle x_q \rangle \sim 0.483$ and for the product form is $\langle x_q \rangle \sim 0.471$, i.e. quite similar but a little bit different from $1/2$. As a simple cross-check we have reobtained those values also from $A^{I=0}_{2,0}(0) = \langle x_q \rangle$ [cf. Eq. (22) with $j = 0$ and Eq. (18)].

A more detailed analysis of the parton distribution can be achieved by using the chiral-even TMD distribution $f_1(x, |\mathbf{k}_\perp|)$; see Eq. (20). In Fig. 7, the TMD distributions calculated within the covariant model by using the different BS amplitudes of Eqs. (37) and (38) are shown. In order to avoid a log plot, $f_1(x, |\mathbf{k}_\perp|)$ has been divided by $G(|\boldsymbol{k}_\perp|) = 1/(1 + |\boldsymbol{k}_\perp|^2/m_\rho^2)^4$ (with $m_\rho = 770$ MeV). Clearly, the product form has a $|\mathbf{k}_\perp|$ falloff faster than the sum form does; i.e. low transverse-momentum partons are favored in the first case.

The analysis of both of the generalized form factors involved in the second moment of the isoscalar pion GPD, i.e. $A^{I=0}_{2,0}(t)$ and $A^{I=0}_{2,2}(t)$ [cf. Eq. (22) with $j = 0$], has to be performed necessarily within the covariant analytic model of Sec. IV. This is obvious if we look at Eq. (17), where the polynomiality imposes a square dependence upon ξ, and therefore one needs a model that covers an extended range for the variable ξ. Indeed, for each value of t, we have first numerically checked the parabolic behavior against ξ, and then we have extracted the coefficients of the parabolic fit getting the values of $A^{I=0}_{2,0}(t)$ and $A^{I=0}_{2,2}(t)$. Figure 8 shows a comparison between (i) recent results from lattice QCD, extrapolated to the physical pion mass [55,56], (ii) our covariant calculations evaluated with both $m_\pi = 0$ and $m_\pi = m_{\rm phys}$ by using the sum and the product form for the BS amplitude [Eqs. (37) and (38)], and (iii) the LFHD result (see Sec. V B) for $A^{I=0}_{2,0}(t)$ only, since this approach at the present stage allows one to perform calculations exclusively for $\xi = 0$. Indeed, the ratios $A^{I=0}_{2,0}(t)/A^{I=0}_{2,0}(0)$ and $A^{I=0}_{2,2}(t)/A^{I=0}_{2,2}(0)$ are presented in order to get rid of the evolution (see Ref. [14] for a detailed discussion of this issue). The lattice calculations are described through a monopole form $1/(1 - t/M^2_{2,i})$, as obtained in Ref. [55] from the analysis of their lattice data, without evolution and with evolution in the $\overline{\rm MS}$ scheme at the scale $\mu = 2$ GeV. In particular, we have used the following values: $M_{2,0} = 1.329 \pm 0.058$ GeV and $M_{2,2} = 0.89 \pm 0.25$ GeV, corresponding to an analysis of the lattice data that satisfies the low-energy theorem, i.e. $A^{I=0}_{2,0}(0) = -4A^{I=0}_{2,2}(0)$. The uncertainties on the previous

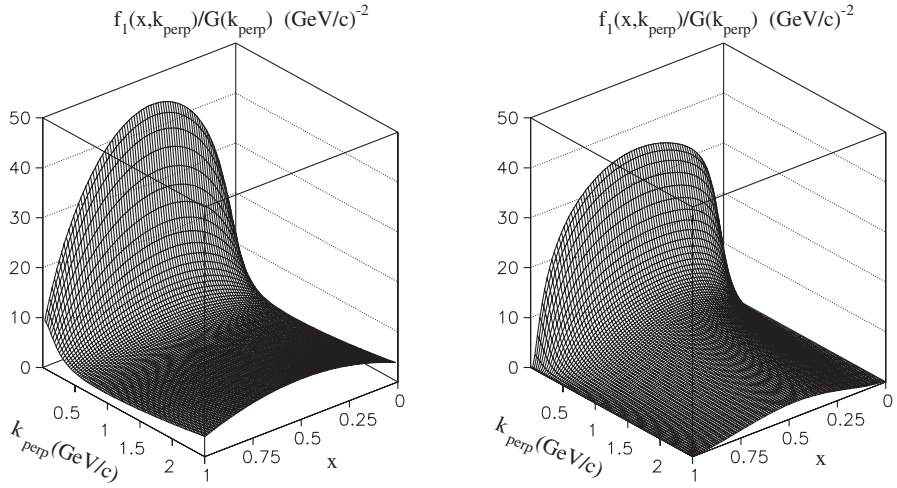

FIG. 7. Transverse-momentum-dependent function $f_1(x, |\boldsymbol{k}_\perp|^2)/G(|\boldsymbol{k}_\perp|)$, with $G(|\boldsymbol{k}_\perp|) = 1/(1 + |\boldsymbol{k}_\perp|^2/m_\rho^2)^4$. Left panel: Sum form of the Bethe-Salpeter amplitude [see Eq. (37)]. Right panel: The same as in the left panel, but for the product form of the Bethe-Salpeter amplitude [see Eq. (38)]. The normalization is given by $\int_0^1 dx \int d\mathbf{k}_\perp f_1(x, |\mathbf{k}_\perp|^2) = 1$, and $k_{\rm perp}$ means $|\mathbf{k}_\perp|$.

masses generate the shaded areas in the left and right panels in Fig. 8.

Unfortunately, (i) the available range of $(-t)$ (we refrained from enlarging the interval as we did in the case of the em form factor, since we do not have experimental data yielding confidence in an arbitrary extension of the monopole fit) and (ii) the large uncertainties in the lattice calculations of $A_{2,2}^{I=0}$ do not allow us to elaborate too much on the comparison between our phenomenological models and the lattice results. On the other hand, for large values of $|t|$ the calculations obtained by using the covariant model with the product form and $m_\pi = 140$ MeV could give some insight on the expected behavior of the lattice calculations, since one could argue that the covariant model with the product form phenomenologically contains to some extent dynamical features typical of QCD, like the one-gluon-exchange dominance at small distances. In order to complete the information, in Table I the values of $A_{2,0}^{I=0}(0)$ and $A_{2,2}^{I=0}(0)$ are shown. It is worth noting that, while the lattice calculations largely fulfill the low-energy theorem, as already mentioned, our calculations do not. Furthermore, it should be pointed out that for small t the disagreement between lattice data and the calculation with the covariant approach to some extent is an expected one, since the mechanism responsible for the confinement is not present in our model, and therefore we have a free propagation of the $q\bar{q}$ pair. A possible solution could be elaborated following the suggestion in Ref. [57], where a covariant model without the disturbing free propagation of the $q\bar{q}$ pair was proposed and applied to the em decays of the vector mesons.

The previous figures have illustrated ''integral'' properties of the pion GPDs, like the em form factor and the generalized ones, or the parton distribution, i.e.

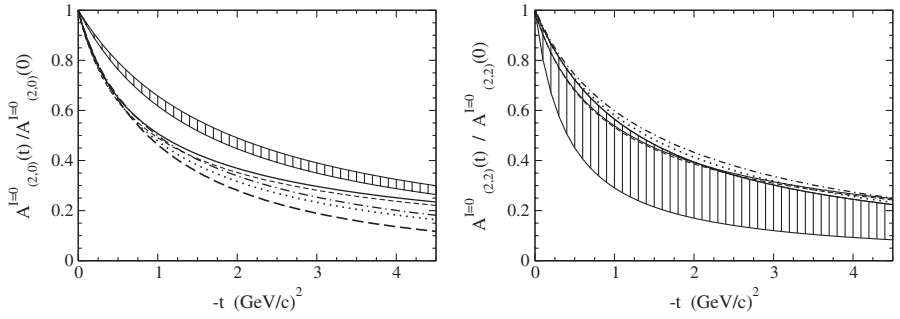

FIG. 8. Left panel: The ratio $A_{2,0}^{I=0}(t)/A_{2,0}^{I=0}(0)$, involving the generalized form factor $A_{2,0}^{I=0}(t)$ that appears in the second moment of the isovector GPD $H^{I=0}$ [cf. Eqs. (17) and (22)] as a function of t. Solid line: Sum form for the pion Bethe-Salpeter amplitude [Eq. (37)] and $m_\pi = 0$. Dashed line: The same as the solid line, but with $m_\pi = 140$ MeV. Dotted-dashed line: Product form for the pion Bethe-Salpeter amplitude [Eq. (38)] and $m_\pi = 0$. Dotted line: The same as the dashed-dotted line, but with $m_\pi = 140$ MeV. Thick long-dashed line: LFHD model (cf. Sec. V B) with a Gaussian pion wave function and the proper Melosh rotations. Shaded area: Results from lattice QCD [55] (see text). Right panel: The same as the left panel, but for $A_{2,2}^{I=0}(t)/A_{2,2}^{I=0}(0)$.

TABLE I. Gravitational form factors at $t = 0$ [cf. Eq. (22) with $j = 0$], obtained (i) within the covariant model of Sec. IV and both the sum and the product form for the BS amplitude [Eqs. (37) and (38)] and (ii) from the lattice data of Ref. [55].

	Sum	Sum	Product	Product	Latt. no evol.	Latt. with $\overline{\text{MS}}$ evol.
	$m_\pi = 0$	$m_\pi = m_{\text{phys}}$	$m_\pi = 0$	$m_\pi = m_{\text{phys}}$	$m_\pi = m_{\text{phys}}$	$m_\pi = m_{\text{phys}}$
$A^{I=0}_{2,0}(0)$	0.4828	0.4833	0.4707	0.4710	0.365	0.261
$A^{I=0}_{2,2}(0)$	−0.0307	−0.0272	−0.0357	−0.0327	−0.092	−0.066

$H^{I=1}(x, 0, 0)$. In the following figures, the isoscalar and isovector GPDs are shown in the plane (x, t) with $-1 \leq x \leq 1$ and $-10\ (\text{GeV}/c)^2 \leq t \leq 0$ but with fixed values for ξ, as dictated by the two phenomenological models, namely, $|\xi| = 1$ for the Mandelstam-inspired model (Sec. V) and $\xi = 0$ for the LFHD model (Sec. V B), respectively. The covariant model (Sec. IV), in its two versions for the momentum dependence [Eqs. (37) and (38)], will be compared to the results for the two phenomenological models that, in some sense, represent two extrema, in the Fock language: The first model is basically related to the nonvalence (ERBL) region, and the second one is related to the valence (DGLAP) domain. In order to cover the whole range of ξ for the given interval of t [i.e. $-10\ (\text{GeV}/c)^2 \leq t \leq 0$], the covariant model has been evaluated by assuming $m_\pi = 0$, as already pointed out. Finally, let us stress that the GPDs are divided by F_{mon}, as in the case of the em form factor, for avoiding a log plot and for emphasizing as many details as possible. In Fig. 9, the results of the covariant symmetric model are shown for

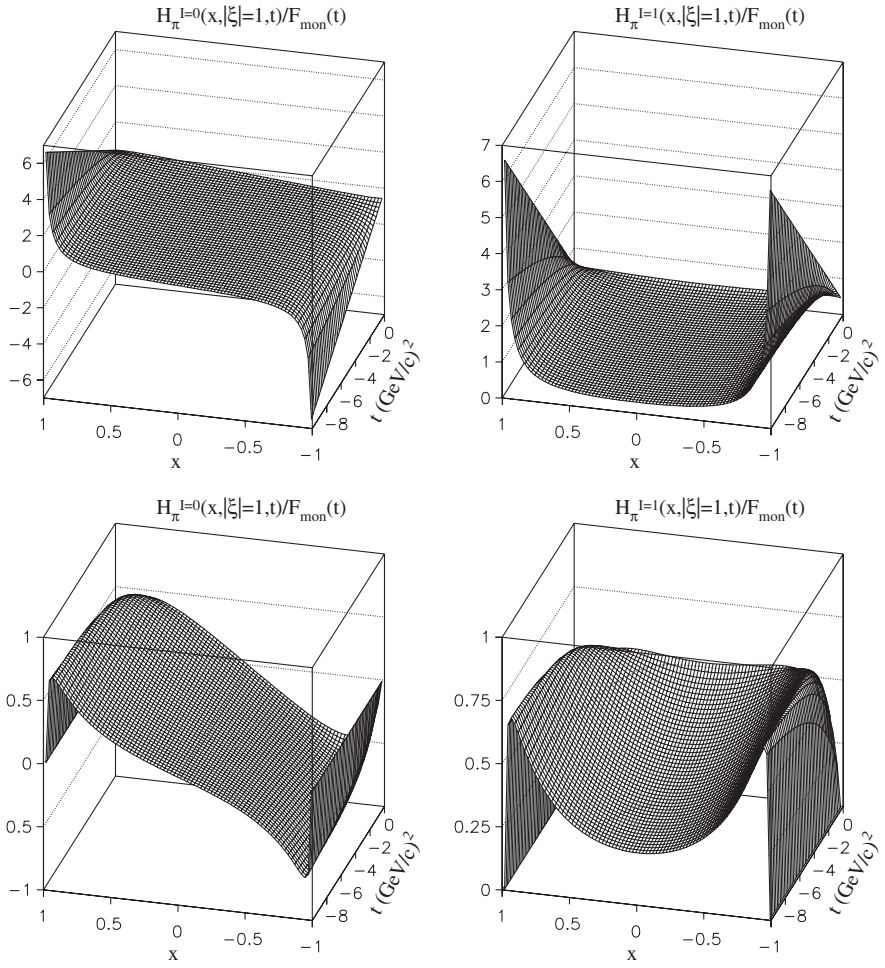

FIG. 9. Upper left panel: Isoscalar no-helicity flip GPD from the covariant symmetric model of Sec. IV with the sum form for the Bethe-Salpeter amplitude [Eq. (37)] at $|\xi| = 1$. The value of ξ is fixed by using $m_\pi = 0$ [cf. Eq. (35)], for the sake of comparison with the microscopic model of Sec. V, whose results are shown in Fig. 10. On the z axis, the ratio with respect to $F_{\text{mon}} = 1/(1 + |t|/m_\rho^2)$ is presented. Upper right panel: The same as in the upper left panel, but for the isovector GPD. Lower panels: The same as in upper panels, but for the product form for the Bethe-Salpeter amplitude [see Eq. (38)].

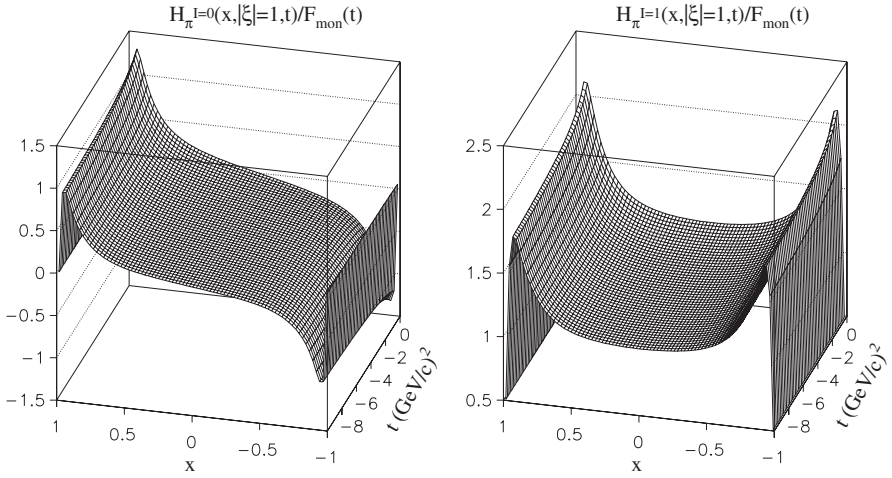

FIG. 10. Left panel: Isoscalar no-helicity flip GPD from the Mandelstam-inspired model of Sec. V at $|\xi| = 1$ (see text). Right panel: the same as in the left panel, but for the isovector GPD.

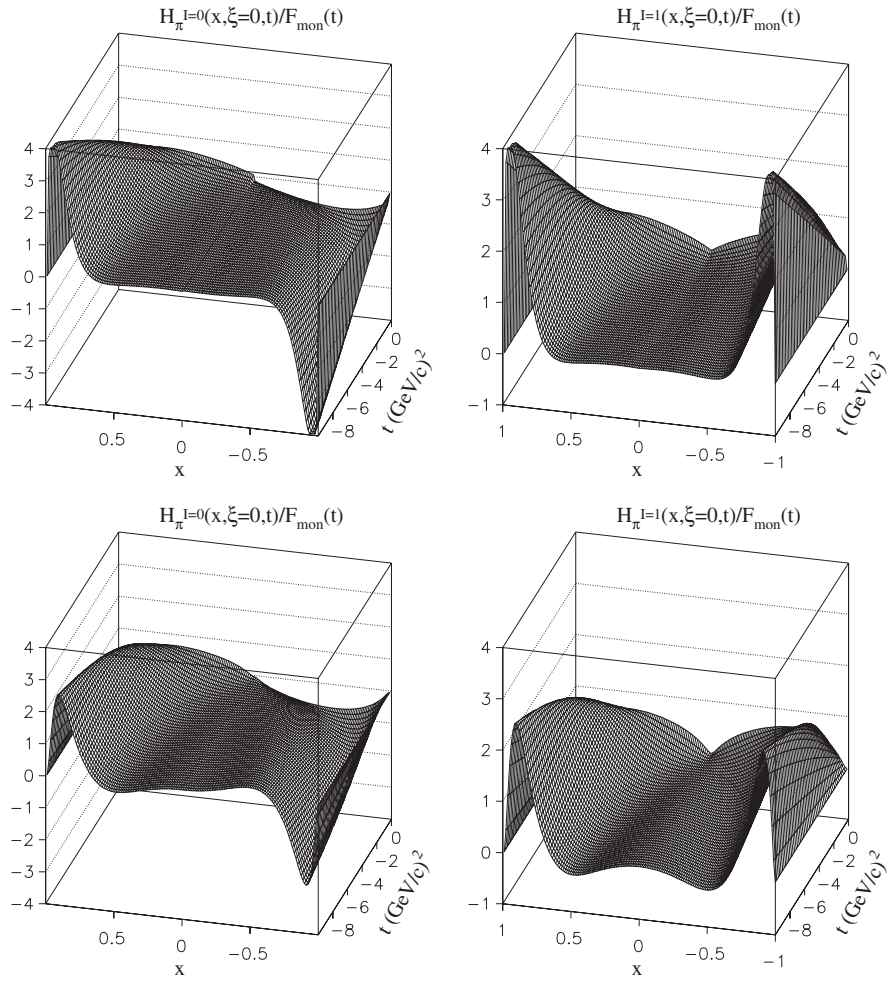

FIG. 11. Upper left panel: Isoscalar no-helicity flip GPD from the covariant symmetric model of Sec. IV, with the sum form for the Bethe-Salpeter amplitude [Eq. (37)] at $\xi = 0$, and $m_\pi = 0$. Upper right panel: The same as in the left panel, but for the isovector GPD. Lower panels: The same as in the upper panels, but for the product form for the Bethe-Salpeter amplitude [Eq. (38)].

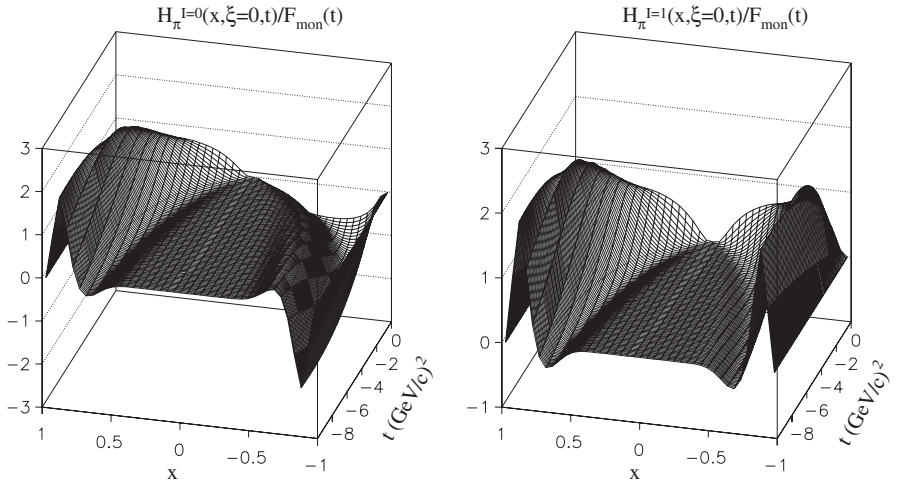

FIG. 12. Left panel: Isoscalar no-helicity flip GPD from the LFHD model of Sec. V B at $\xi = 0$ (see text). Right panel: The same as in the left panel, but for the isovector GPD.

$|\xi| = 1$, in order to be compared with the calculations performed by using the Mandelstam-inspired model, presented in Fig. 10. We remind the reader that the phenomenological model has a photon-quark vertex dressed by a microscopical VMD, as discussed in Sec. V.

In Fig. 11, the no-helicity flip GPDs of the covariant symmetric model are shown for $\xi = 0$, allowing a comparison with the calculations performed by using the LFHD model, presented in Fig. 12. For $\xi = 0$, where only the valence component is acting and $|x| = x_q$, a nice feature stemming from the figures of both isoscalar and isovector GPDs is shared by all of the presented models: In the limit of large $|t|$ the collinearity clearly emerges, as shown by the migration of the maximum (minimum) value from $|x| \simeq 1/2$ for $t = 0$ toward $|x| \sim 1$ for $|t| \to \infty$. Such a behavior can be easily understood in the LFHD model, since nonvanishing contributions to GPD [cf. Eq. (65)] can be obtained if $\boldsymbol{\kappa}'_\perp$ in Eq. (59) does not depend too much from $\boldsymbol{\Delta}_\perp$, namely, $x \sim 1$ (notice that for x exactly 1, the free mass blows up and the wave functions become vanishing, as well as GPDs). Correspondingly, for $|\xi| = 1$, where only the nonvalence component is acting, the relevance of the x region around ± 1 can be explained by the pair-production mechanism. For simplicity, let us consider large values of $|t|$ that amount to large values of $\Delta^+ = \Delta_z$ (recall that in the Breit frame $\Delta^0 = 0$). Then, using $\Delta^+ = k_q^+ + k_{\bar{q}}^+ = k_{zq} + k_{z\bar{q}} \sim 2k_{zq} \geq 0$ (given our choice for the sign of Δ^+) and the fact that each quark in the pair is almost on its mass shell, we can approximate $2k^+ = k_q^+ - k_{\bar{q}}^+ \sim 2E_q = 2\sqrt{m^2 + |\vec{k}_q|^2}$. Thus, one can see that, when $\xi = -1$, x becomes close to 1 for $\Delta_z \gg m$, since $x = k^+/P^+ = 2k^+/\Delta^+ \sim E_q/k_{zq} \to 1$. The case $x = -1$ can be obtained for $\Delta^+ \leq 0$.

Finally, in Fig. 13, the isovector GPD, evaluated within the covariant model adopting the product form of Eq. (38) and $m_\pi = 0$, is shown for the case $x = |\xi|$ and $0 \geq t \geq -10\ (GeV/c)^2$. This kinematical region, where the transition from DGLAP to ERBL regimes occurs, should be relevant for the experimental studies of the single spin asymmetry (see, e.g., the discussion in [4,58]). Let us notice that in our covariant analytic model the GPD is continuous at $x = |\xi|$.

From the 3D plots, one can see that the covariant model, in the version with the product form for the momentum-dependent part of the BS amplitude, is able to reproduce

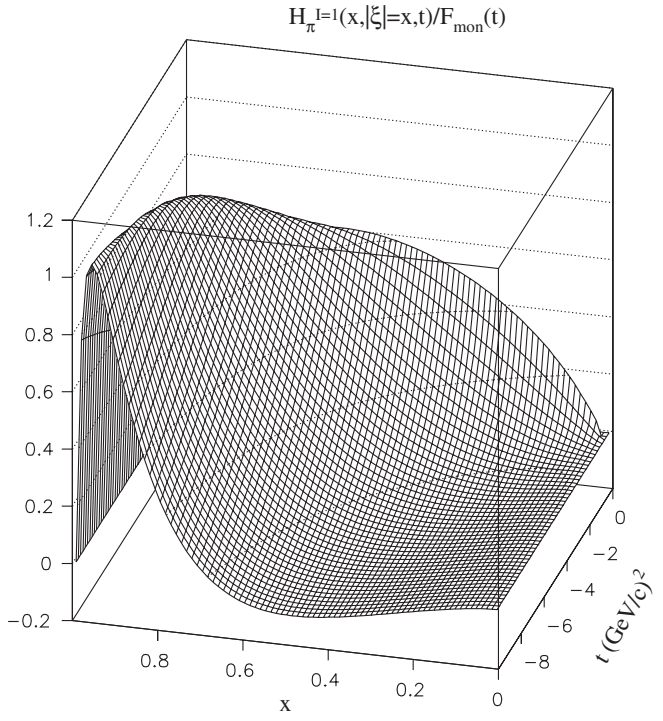

FIG. 13. Isovector no-helicity flip GPD from the covariant symmetric model of Sec. IV, with the product form for the Bethe-Salpeter amplitude [Eq. (38)] at $|\xi| = x$, and $m_\pi = 0$.

quite satisfactorily the GPDs evaluated within the two phenomenological models, the Mandelstam-inspired and the LFHD ones, and therefore one could argue that it contains the main ingredients for a realistic description of the constituents inside the pion. In view of this, it appears challenging to test the covariant model (or its refinements [59] based on the Nakanishi representation; see, e.g., [37], for recent applications to a bosonic system) of the BS amplitude, in comparison with experimental data, whose analysis requires the knowledge of the pion GPDs.

VII. CONCLUSION

In this paper, we have investigated the no-helicity flip generalized parton distributions of the pion by using three models, based on a description of the pion where constituent quarks with masses between 200 and 250 MeV are considered. In particular, we have evaluated the isoscalar and isovector GPDs adopting a covariant, analytic model and two light-front phenomenological models. It is important to notice that the first model, based on 4D *Ansätze* for the Bethe-Salpeter amplitudes, allows us to explore the whole kinematical domain of the three variables x, ξ, and t upon which the GPDs depend, while the others two are, presently, constrained to a given value of ξ. The second model, the Mandelstam-inspired model of Sec. V, is a natural extension of the approach proposed in Ref. [22] for a successful investigation of the em form factor of the pion in both the space- and timelike regions. The main features of the model are (i) a microscopical vector-meson model dressing for the quark-photon vertex and (ii) proper *Ansätze* for the 3D LF projection of the BS amplitudes of both pion and vector mesons, taken as the eigenfunctions of a LF square mass operator [43]. As in Ref. [22], the assumption $m_\pi = 0$ is added, and this simplification allows calculations of the GPDs only for the value $|\xi| = 1$ [cf. Eq. (35)]; namely, the nonvalence region covers the whole range $1 \geq x \geq -1$.

On the contrary, the LFHD model of Sec. V B is based on a Poincaré covariant description of the pion, with a proper treatment of the spin wave functions, due to the presence of the Melosh rotations. The momentum part of the pion wave function is given by a Gaussian function that contains the dynamical input of the model through two adjusted parameters. A bare quark-photon vertex is assumed. It is worth noting that the model yields a description of the GPDs for $\xi = 0$; i.e. the valence region can be investigated.

The covariant symmetric model of Sec. IV, based on a Mandelstam formula for matrix elements of the operators yielding the isoscalar and isovector GPDs, allows us to have close expressions for the physical quantities, since analytic forms for the momentum-dependent part of the Bethe-Salpeter amplitude are adopted and a bare quark-photon vertex is assumed as well. Such a covariant model can be applied for any value of x, ξ, and t and therefore can be used for interpolating between the two phenomenological models. A peculiar feature is given by the presence of instantaneous terms, in both the valence and the nonvalence regions, since we fully take into account the analytic structure of the BS amplitude.

The comparison with the em form factor (Fig. 3) suggests that the covariant model with a sum form of the BS amplitude has a nonrealistic increasing behavior with respect to $F_{\rm mon}$, for large $|t|$, which leads to a divergent density at short distances, while the version with a product form together with the LFHD model decreases more rapidly than $F_{\rm mon}$. Finally, the Mandelstam-inspired model and the lattice results (red curve in Fig. 3), arbitrarily extended from $t = -4$ $(\mathrm{GeV}/c)^2$ to $t = -10$ $(\mathrm{GeV}/c)^2$, given the analytic form proposed in Ref. [51] for extrapolating the lattice data to the physical m_π, show a moderate decreasing with respect to $F_{\rm mon}$, for large $|t|$. Such a comparison for the em form factor and the analysis of the parton distribution in Fig. 6 point to the relevance of the behavior of the pion valence function (or better the momentum part of the BS amplitude) for large transverse momentum. In particular, the product form, that has a behavior at large transverse momentum $|\mathbf{k}_\perp|$ compatible with the one suggested by the one-gluon-exchange dominance (see, e.g., [37]), seems to give a consistent description of both the tail of the em form factor and the end-point falloff of the parton distribution. With respect to this finding, more details can be gained from the investigation of the chiral-even transverse-momentum-dependent distribution, as shown in Fig. 7.

Another important step in the characterization of the covariant model is given by the comparison of the generalized form factors with the lattice results. For the present, the comparison is restricted to the gravitational form factors $A^{I=0}_{2,0}(t)$ and $A^{I=0}_{2,2}(t)$ that appear in the second moment of the isovector GPD $H^{I=0}$ [cf. Eqs. (17) and (22)]. Indeed, for $A^{I=0}_{2,0}(t)$ we have presented results from both our covariant model and the LFHD approach, while for $A^{I=0}_{2,2}(t)$ only the covariant calculations are available (let us remind the reader that calculations with $\xi \neq 0$ are necessary for disentangling both form factors). Unfortunately, since lattice data have been obtained in a t interval not too wide and are affected by large uncertainties, one cannot yet draw stringent conclusions from the comparison shown in Fig. 8. However, the encouraging agreement between model calculations and lattice data for both ratios $A^{I=0}_{0,2}(t)/A^{I=0}_{0,2}(0)$ and $A^{I=0}_{2,2}(t)/A^{I=0}_{2,2}(0)$ suggests to extend our analysis also to the spin-flip GPDs, since lattice results are available for the lowest moments [56], in order to explore the onset of the dominance of a one-gluon-exchange mechanism for a light hadron.

To complete our analysis, we have studied the GPDs in the (x, t) plane for fixed values of ξ, i.e. $|\xi| = 0, 1, x$. These values are representative of different, interesting cases. The

first one, $\xi = 0$, involves contributions to GPDs only in the valence region, while the second one involves contributions only from the nonvalence one. Finally, the case $|\xi| = x$ illustrates the transition from the DGLAP region to the ERBL one. The covariant model can explore the whole 3D space of the variables (x, ξ, t), and it is compared with the LFHD model for $\xi = 0$ and with the Mandelstam-inspired model for $|\xi| = 1$, while for $|\xi| = x$ it shows a smooth transition from the DGLAP region to the ERBL one, given the continuity of the model. It should be pointed out that the covariant model with the product form for the Bethe-Salpeter amplitude exhibits an overall agreement with the Mandelstam-inspired model, for $|\xi| = 1$, and with the LFHD model, for $\xi = 0$. Therefore, from these findings one could conjecture that the general shape, illustrated by the previous covariant model and the phenomenological ones, is a typical feature of the pion GPDs, dictated from both kinematical arguments (cf. the discussion at the end of Sec. VI) and the dynamical input reflected by the proper falloff of the momentum distribution (cf. the one-gluon-exchange dominance at short distances).

Further analyses, to make more and more realistic the models presented in this paper, are in progress.

ACKNOWLEDGMENTS

This work was partially supported by the Brazilian agencies CNPq and FAPESP and by Ministero della Ricerca Scientifica e Tecnologica. It is also part of the Research Infrastructure Integrating Activity "Study of Strongly Interacting Matter" (acronym HadronPhysics2, Grant Agreement No. 227431) under the Seventh Framework Program of the European Community. T. F. acknowledges the hospitality of the Dipartimento di Fisica, Università di Roma "Tor Vergata" and of Istituto Nazionale di Fisica Nucleare, Sezione Tor Vergata and Sezione di Roma.

APPENDIX A: KINEMATICS

Following the notations of Fig. 1, where $\Delta^+ \geq 0$, one obtains from Eq. (1) that $0 \geq \xi$.

In the valence region, for a quark, one has (i) in the initial state, $p^+ \geq k^+ - \Delta^+/2 \geq 0$, i.e. $P^+ \geq k^+ \geq \Delta^+/2$ (notice that necessarily the spectator constituent is an antiquark, since $0 \geq k^+ - P^+$) and then $1 \geq x \geq -\xi$; (ii) in the final state, $p'^+ \geq k^+ + \Delta^+/2 \geq 0$, i.e. $P^+ \geq k^+ \geq -\Delta^+/2$, and then $1 \geq x \geq \xi$. Therefore in the valence region, one gets the interval $1 \geq x \geq -\xi$, and given our choice for ξ one has $1 \geq x \geq |\xi|$.

For an antiquark in the initial pion, the four-momentum is $k + \Delta/2$, while the spectator quark has four-momentum $k + P$. In the final pion, the antiquark four-momentum is $k - \Delta/2$. The antiquark plus components are negative both in the initial and in the final pion. Therefore (i) $p^+ \geq -(k^+ + \Delta^+/2) \geq 0$ that leads to $\xi \geq x \geq -1$ and (ii) $p'^+ \geq -(k^+ - \Delta^+/2) \geq 0$, i.e. $-\xi \geq x \geq -1$. In summary, for an antiquark in the valence region, one finds $-|\xi| \geq x \geq -1$.

In the nonvalence region, one has to deal with a $q\bar{q}$ production, i.e. $0 > k^+ - \Delta^+/2$ and $k^+ + \Delta^+/2 > 0$ (see Fig. 2), and those constraints translate into $\xi < x < -\xi$. The $q\bar{q}$ annihilation is prevented by the choice of a positive Δ^+. In order to have general extrema, holding for both positive and negative Δ^+, one can write $|\xi| > x > -|\xi|$.

APPENDIX B: INTEGRATION ON k^-

In this appendix, the no-helicity flip GPD for the symmetric covariant models (see Sec. IV) are calculated using Eq. (40) and the momentum-dependent part of the BS amplitude, given by Eq. (37) or (38).

The evaluation of the trace in Eq. (41) can be simplified according to the decomposition of the Dirac propagator shown in Eq. (42) and by recalling that $[\gamma^+]^2 = 0$. By introducing the variable $\kappa = P - k$, one has

$$\begin{aligned}
\mathrm{Tr}[\mathcal{O}^+(\kappa^-)] &= \mathrm{Tr}\{(\not{\kappa} + m)(\not{p}' - \not{\kappa} + m)\gamma^+(\not{p} - \not{\kappa} + m)\} \\
&= \mathrm{Tr}[\mathcal{O}^+(\kappa^-_{\mathrm{on}})] + \frac{(\kappa^- - \kappa^-_{\mathrm{on}})}{2}\,\mathrm{Tr}\{\gamma^+[(\not{p}' - \not{\kappa})_{\mathrm{on}} + m]\gamma^+[(\not{p} - \not{\kappa})_{\mathrm{on}} + m]\} \\
&= -4\{\kappa^+[(p' - \kappa)_{\mathrm{on}} \cdot (p - \kappa)_{\mathrm{on}} - m^2] - (p'^+ - \kappa^+)[\kappa_{\mathrm{on}} \cdot (p - \kappa)_{\mathrm{on}} - m^2] \\
&\quad - (p^+ - \kappa^+)[(p' - \kappa)_{\mathrm{on}} \cdot \kappa_{\mathrm{on}} - m^2]\} + 4(\kappa^- - \kappa^-_{\mathrm{on}})(p'^+ - \kappa^+)(p^+ - \kappa^+),
\end{aligned} \tag{B1}$$

where

$$\mathrm{Tr}[\mathcal{O}^+(\kappa^-_{\mathrm{on}})] = \mathrm{Tr}\{(\not{\kappa}_{\mathrm{on}} + m)[(\not{p}' - \not{\kappa})_{\mathrm{on}} + m]\gamma^+[(\not{p} - \not{\kappa})_{\mathrm{on}} + m]\}. \tag{B2}$$

After performing the scalar products, one gets

$$\mathrm{Tr}[\mathcal{O}^+(\kappa^-)] = 4p'^+p^+\kappa^-_{\mathrm{on}} - \kappa^+|\boldsymbol{\Delta}_\perp|^2 + 2\Delta^+\boldsymbol{\kappa}_\perp \cdot \boldsymbol{\Delta}_\perp + 4(\kappa^- - \kappa^-_{\mathrm{on}})(p'^+ - \kappa^+)(p^+ - \kappa^+). \tag{B3}$$

Given the simple expression adopted for the momentum dependence of the BS amplitude [see Eqs. (37) and (38)], the analytic integration on k^- can be easily performed in Eq. (40).

By using the LF variables (i.e. $d^4\kappa \to d\kappa^+ d\kappa^- d\boldsymbol{\kappa}_\perp/2$), one obtains

$$H^u(x,\xi,t) = -\imath N_c \mathcal{R} \int \frac{d\kappa^+ d\kappa^- d\boldsymbol{\kappa}_\perp}{4(2\pi)^4} \delta[P^+(1-x)-\kappa^+] \frac{\mathrm{Tr}[\mathcal{O}^+(\kappa^-)]}{\kappa^+(p^+-\kappa^+)(p'^+-\kappa^+)} \frac{1}{(\kappa^- - \kappa^-_{\rm on} + i\frac{\epsilon}{\kappa^+})} \times \frac{1}{[p^- - \kappa^- - (p-\kappa)^-_{\rm on} + i\frac{\epsilon}{(p^+-\kappa^+)}]} \frac{1}{[p'^- - \kappa^- - (p'-\kappa)^-_{\rm on} + i\frac{\epsilon}{(p'^+-\kappa^+)}]} \Lambda(\kappa,p')\Lambda(\kappa,p), \tag{B4}$$

where

$$\kappa^-_{\rm on} = \frac{m^2 + |\boldsymbol{\kappa}_\perp|^2}{\kappa^+}, \qquad (p-\kappa)^-_{\rm on} = \frac{m^2 + |\boldsymbol{p}_\perp - \boldsymbol{\kappa}_\perp|^2}{(p^+-\kappa^+)}, \qquad (p'-\kappa)^-_{\rm on} = \frac{m^2 + |\boldsymbol{p}'_\perp - \boldsymbol{\kappa}_\perp|^2}{(p'^+-\kappa^+)}. \tag{B5}$$

In the integration over the minus component κ^-, one faces with the following six poles (coming from the BS amplitudes and the Dirac propagators):

$$\kappa^-_{1(2)} = \kappa^-_{{\rm on}(R)} - i\frac{\epsilon}{\kappa^+}, \qquad \kappa^-_{3(4)} = p^- - (p-\kappa)^-_{{\rm on}(R)} + i\frac{\epsilon}{(p^+-\kappa^+)}, \qquad \kappa^-_{5(6)} = p'^- - (p'-\kappa)^-_{{\rm on}(R)} + i\frac{\epsilon}{(p'^+-\kappa^+)}, \tag{B6}$$

where κ^-_R, $(p-\kappa)^-_R$, and $(p'-\kappa)^-_R$ can be obtained from the corresponding quantities in Eq. (B5) by substituting $m \to m_R$. Notice that κ^-_2 can appear both as a single and as a double pole.

It is easily seen that the analytic integral (B4) is not vanishing only if $p'^+ \geq \kappa^+ \geq 0$. Furthermore we can recognize two subintervals: (i) $p^+ \geq \kappa^+ \geq 0$, or the valence region, and (ii) $p'^+ \geq \kappa^+ \geq p^+$, the nonvalence region. Let us stress that Eq. (B4) is vanishing for $x < -|\xi|$, since in this case $\kappa^+ = P^+(1-x) > P^+(1+|\xi|) = p'^+$.

In the valence region, only the poles κ^-_1 and κ^-_2 belong to the lower semiplane. In the nonvalence region, only κ^-_5 and κ^-_6 belong to the upper semiplane.

To obtain the no-helicity flip GPD in the valence region, let us integrate over κ^- closing the contour in the lower semiplane. The contribution from κ^-_1 reads as follows:

$$H^u_{(v){\rm on}}(x,\xi,t) = -\frac{N_c\mathcal{R}}{4(2\pi)^3} \int d\boldsymbol{\kappa}_\perp \int_0^{p^+} d\kappa^+ \frac{\delta[P^+(1-x)-\kappa^+]}{\kappa^+(p^+-\kappa^+)(p'^+-\kappa^+)} \mathrm{Tr}[\mathcal{O}^+(\kappa^-_{\rm on})] \frac{\Lambda(\kappa,p)|_{\kappa^-_{\rm on}}}{[p^- - \kappa^-_{\rm on} - (p-\kappa)^-_{\rm on}]} \times \frac{\Lambda(\kappa,p')|_{\kappa^-_{\rm on}}}{[p'^- - \kappa^-_{\rm on} - (p'-\kappa)^-_{\rm on}]}, \tag{B7}$$

where for the sum form [Eq. (37)] one has

$$\Lambda(\kappa,p)|_{\kappa_{\rm on}} = C_1 \left\{ \frac{1}{(p^+-\kappa^+)[p^- - \kappa^-_{\rm on} - (p-\kappa)^-_R]} + \frac{1}{\kappa^+(\kappa^-_{\rm on} - \kappa^-_R)} \right\} \tag{B8}$$

and for the product form [Eq. (38)] one has

$$\Lambda(\kappa,p)|_{\kappa_{\rm on}} = C_2 \frac{1}{(p^+-\kappa^+)[p^- - \kappa^-_{\rm on} - (p-\kappa)^-_R]} \frac{1}{\kappa^+(\kappa^-_{\rm on} - \kappa^-_R)}. \tag{B9}$$

For the sum form, the pole κ^-_R generates a contribution as a single pole and a contribution as a double pole.

The single-pole contribution is given by

$$H^u_{(v)1}(x,\xi,t) = -\frac{N_c\mathcal{R}}{4(2\pi)^3} C_1^2 \int d\boldsymbol{\kappa}_\perp \int_0^{p^+} d\kappa^+ \frac{\delta[P^+(1-x)-\kappa^+]}{(\kappa^+)^2(p^+-\kappa^+)(p'^+-\kappa^+)} \mathrm{Tr}[\mathcal{O}^+(\kappa^-_R)] \frac{1}{(\kappa^-_R - \kappa^-_{\rm on})} \times \frac{1}{[p^- - \kappa^-_R - (p-\kappa)^-_{\rm on})][p'^- - \kappa^-_R - (p'-\kappa)^-_{\rm on}]} \left\{ \frac{1}{(p^+-\kappa^+)[p^- - \kappa^-_R - (p-\kappa)^-_R]} + \frac{1}{(p'^+-\kappa^+)[p'^- - \kappa^-_R - (p'-\kappa)^-_R]} \right\}, \tag{B10}$$

and the double-pole contribution is given by

$$H^u_{(v)2}(x,\xi,t) = -\frac{N_c\mathcal{R}}{4(2\pi)^3}C_1^2\int d\boldsymbol{\kappa}_\perp\int_0^{p^+}d\kappa^+\frac{\delta[P^+(1-x)-\kappa^+]}{(\kappa^+)^3(p^+-\kappa^+)(p'^+-\kappa^+)}\frac{d}{d\kappa^-}\Big\{\frac{\mathrm{Tr}[\mathcal{O}^+(\kappa^-)]}{(\kappa^- - \kappa^-_{\rm on})} \times \frac{1}{[p^- - \kappa^- - (p-\kappa)^-_{\rm on})][p'^- - \kappa^- - (p'-\kappa)^-_{\rm on}]}\Big\}\Big|_{\kappa^-_R}. \tag{B11}$$

For the product form, the pole κ^-_R generates only a double-pole contribution, given by

$$H^u_{(v)2'}(x,\xi,t) = -\frac{N_c\mathcal{R}}{4(2\pi)^3}C_2^2\int d\boldsymbol{\kappa}_\perp\int_0^{p^+}d\kappa^+\frac{\delta[P^+(1-x)-\kappa^+]}{(\kappa^+)^3(p^+-\kappa^+)^2(p'^+-\kappa^+)^2}\frac{d}{d\kappa^-}\Big\{\frac{\mathrm{Tr}[\mathcal{O}^+(\kappa^-)]}{(\kappa^- - \kappa^-_{\rm on})} \times \frac{1}{[p^- - \kappa^- - (p-\kappa)^-_{\rm on})][p'^- - \kappa^- - (p'-\kappa)^-_{\rm on}]}\frac{1}{[p^- - \kappa^- - (p-\kappa)^-_R)][p'^- - \kappa^- - (p'-\kappa)^-_R]}\Big\}\Big|_{\kappa^-_R}. \tag{B12}$$

The contribution in the nonvalence region can be evaluated by considering the poles κ^-_5 and κ^-_6. In particular, the contribution from κ^-_5 has the same form for both choices of the BS amplitudes, i.e.

$$H^u_{(nv)5}(x,\xi,t) = -\frac{N_c\mathcal{R}}{4(2\pi)^3}\int d\boldsymbol{\kappa}_\perp\int_{p^+}^{p'^+}d\kappa^+\frac{\delta[P^+(1-x)-\kappa^+]}{\kappa^+(p^+-\kappa^+)(p'^+-\kappa^+)} \times \frac{\mathrm{Tr}[\mathcal{O}^+(p'^- - (p'-\kappa)^-_{\rm on})]\Lambda(\kappa,p')|_{p'^- - (p'-\kappa)^-_{\rm on}}\Lambda(\kappa,p)|_{p'^- - (p'-\kappa)^-_{\rm on}}}{[p'^- - (p'-\kappa)^-_{\rm on} - \kappa^-_{\rm on}][p^- - p'^- + (p'-\kappa)^-_{\rm on} - (p-\kappa)^-_{\rm on}]}, \tag{B13}$$

while the contributions from κ^-_6, reads differently for the sum form, viz.,

$$H^u_{(nv)6}(x,\xi,t) = -\frac{N_c\mathcal{R}}{4(2\pi)^3}C_1\int d\boldsymbol{\kappa}_\perp\int_{p^+}^{p'^+}d\kappa^+\frac{\delta[P^+(1-x)-\kappa^+]}{\kappa^+(p^+-\kappa^+)(p'^+-\kappa^+)^2}\frac{1}{[p'-\kappa)^-_R - (p'-\kappa)^-_{\rm on}]} \times \frac{\mathrm{Tr}[\mathcal{O}^+(p'^- - (p'-\kappa)^-_R)]}{[(p'^- - (p'-\kappa)^-_R - \kappa^-_{\rm on}]}\frac{\Lambda(\kappa,p)|_{p'^- - (p'-\kappa)^-_R}}{[p^- - p'^- + (p'-\kappa)^-_R - (p-\kappa)^-_{\rm on}]} \tag{B14}$$

and for the product form, viz.,

$$H^u_{(nv)6'}(x,\xi,t) = -\frac{N_c\mathcal{R}}{4(2\pi)^3}C_2\int d\boldsymbol{\kappa}_\perp\int_{p^+}^{p'^+}d\kappa^+\frac{\delta[P^+(1-x)-\kappa^+]}{(\kappa^+)^2(p^+-\kappa^+)(p'^+-\kappa^+)^2}\,\mathrm{Tr}[\mathcal{O}^+(p'^- - (p'-\kappa)^-_R)] \times \frac{1}{[(p'^- - (p'-\kappa)^-_R - \kappa^-_{\rm on}][(p'-\kappa)^-_R - (p'-\kappa)^-_{\rm on}]}\frac{1}{[p^- - p'^- + (p'-\kappa)^-_R - (p-\kappa)^-_{\rm on}]} \times \frac{\Lambda(\kappa,p)|_{p'^- - (p'-\kappa)^-_R}}{[(p'^- - (p'-\kappa)^-_R - \kappa^-_R]}. \tag{B15}$$

In summary, for the sum form one has

$$\begin{aligned}H^u(x,\xi,t) = {}& \theta(x-|\xi|)\theta(1-x)[H^u_{(v)\rm on}(x,\xi,t) \\ & + H^u_{(v)1}(x,\xi,t) + H^u_{(v)2}(x,\xi,t)] \\ & + \theta(|\xi|-x)\theta(|\xi|+x)[H^u_{(nv)5}(x,\xi,t) \\ & + H^u_{(nv)6}(x,\xi,t)],\end{aligned} \tag{B16}$$

with $H^u_{(nv)6}$ given by Eq. (B14), while for the product form one gets

$$\begin{aligned}H^u(x,\xi,t) = {}& \theta(x-|\xi|)\theta(1-x)[H^u_{(v)\rm on}(x,\xi,t) \\ & + H^u_{(v)2'}(x,\xi,t)] + \theta(|\xi|-x)\theta(|\xi|+x) \\ & \times [H^u_{(nv)5}(x,\xi,t) + H^u_{(nv)6'}(x,\xi,t)],\end{aligned} \tag{B17}$$

with $H^u_{(nv)6'}$ given by Eq. (B15).

APPENDIX C: ELECTROMAGNETIC FORM FACTOR

The pion electromagnetic form factor is defined by

$$\begin{aligned}F_\pi(t) &= \frac{1}{2P^+}\langle\pi^+(p')|J(0)\cdot n|\pi^+(p)\rangle \\ &= \int_{-1}^1 dx H^{I=1}(x,\xi,t) \\ &= \frac{1}{2}\int_{-\infty}^{\infty}dx\int\frac{dz^-}{2\pi}e^{ixP^+z^-} \\ &\quad\times\langle\pi^+(p')|\bar\psi_q\Big(-\frac{1}{2}z\Big)\gamma\cdot n\tau_3\psi_q\Big(\frac{1}{2}z\Big)|\pi^+(p)\rangle|_{\vec z=0},\end{aligned} \tag{C1}$$

where the range of x has been extended from $[-1,1]$ to $[-\infty,\infty]$, since $H^{I=1}(x,\xi,t)$ is vanishing outside the support $[-1,1]$, given the presence of the delta function in Eq. (40) and the kinematical relations in Eq. (1) (see, e.g., [1,4]).

[1] X.-D. Ji, J. Phys. G **24**, 1181 (1998); Annu. Rev. Nucl. Part. Sci. **54**, 413 (2004).

[2] A. V. Radyushkin, *At the Frontier of Particle Physics/ Handbook of QCD*, edited by M. Shifman (World Scientific, Singapore, 2001), p. 1037.

[3] K. Goeke, M. V. Polyakov, and M. Vanderhaeghen, Prog. Part. Nucl. Phys. **47**, 401 (2001).

[4] M. Diehl, Phys. Rep. **388**, 41 (2003).

[5] A. V. Belitsky and A. V. Radyushkin, Phys. Rep. **418**, 1 (2005).

[6] S. Boffi and B. Pasquini, Riv. Nuovo Cimento Soc. Ital. Fis. **30**, 387 (2007).

[7] M. V. Polyakov and C. Weiss, Phys. Rev. D **60**, 114017 (1999).

[8] B. C. Tiburzi and G. A. Miller, Phys. Rev. D **65**, 074009 (2002); **67**, 013010 (2003); **67**, 113004 (2003).

[9] A. Mukherjee, I. V. Musatov, H. C. Pauli, and A. V. Radyushkin, Phys. Rev. D **67**, 073014 (2003).

[10] F. Bissey, J. R. Cudell, J. Cugnon, J. P. Lansberg, and P. Stassart, Phys. Lett. B **587**, 189 (2004).

[11] S. Noguera, L. Theussel, and V. Vento, Eur. Phys. J. A **20**, 483 (2004).

[12] M. Diehl, A. Manashov, and A Schäfer, Phys. Lett. B **622**, 69 (2005).

[13] C.-R. Ji, Y. Mishchenko, and A. Radyushkin, Phys. Rev. D **73**, 114013 (2006).

[14] W. Broniowski, E. R. Arriola, and K. Golec-Biernat, Phys. Rev. D **77**, 034023 (2008); W. Broniowski and E. R. Arriola, arXiv:0901.3336.

[15] W. Broniowski and E. R. Arriola, Phys. Rev. D **78**, 094011 (2008).

[16] A. Van Dyck, T. Van Cauteren, J. Ryckebusch, and B. C. Metsch, Phys. Lett. B **662**, 413 (2008).

[17] B. D. Keister and W. N. Polyzou, Adv. Nucl. Phys. **20**, 225 (1991).

[18] S. J. Brodsky, H. C. Pauli, and S. S. Pinsky, Phys. Rep. **301**, 299 (1998).

[19] J. Carbonell, B. Desplanques, V. A. Karmanov, and J. F. Mathiot, Phys. Rep. **300**, 215 (1998).

[20] S. Mandelstam, Proc. R. Soc. A **233**, 248 (1955).

[21] J. P. B. C. de Melo, T. Frederico, E. Pace, and G. Salmè, Nucl. Phys. **A707**, 399 (2002).

[22] J. P. B. C. de Melo, T. Frederico, E. Pace, and G. Salmè, Phys. Lett. B **581**, 75 (2004); Phys. Rev. D **73**, 074013 (2006).

[23] S. J. Brodsky, M. Diehl, and D. S. Hwang, Nucl. Phys. **B596**, 99 (2001).

[24] M. Diehl, T. Feldmann, R. Jakob, and P. Kroll, Nucl. Phys. **B596**, 33 (2001); **B605**, 647(E) (2001).

[25] T. Frederico and G. A. Miller, Phys. Rev. D **45**, 4207 (1992); **50**, 210 (1994).

[26] V. N. Gribov and L. N. Lipatov, Sov. J. Nucl. Phys. **15**, 438 (1972); **15**, 675 (1972); G. Altarelli and G. Parisi, Nucl. Phys. **B126**, 298 (1977); Yu. L. Dokshitzer, Sov. Phys. JETP **46**, 641 (1977).

[27] A. V. Efremov and A. V. Radyushkin, Phys. Lett. **94B**, 245 (1980).

[28] G. P. Lepage and S. J. Brodsky, Phys. Rev. D **22**, 2157 (1980).

[29] J. F. Donoghue and H. Leutwyler, Z. Phys. C **52**, 343 (1991).

[30] R. Jakob, P. J. Mulders, and J. Rodrigues, Nucl. Phys. **A626**, 937 (1997).

[31] D. S. Hwang and D. S. Kim, Phys. Lett. B **662**, 123 (2008).

[32] B. Pasquini, S. Cazzaniga, and S. Boffi, Phys. Rev. D **78**, 034025 (2008), and references therein.

[33] F. M. Lev, E. Pace, and G. Salmè, Nucl. Phys. **A641**, 229 (1998); Phys. Rev. C **62**, 064004 (2000).

[34] J. P. C. B. de Melo, H. W. L. Naus, and T. Frederico, Phys. Rev. C **59**, 2278 (1999).

[35] B. L. G. Bakker, H.-M. Choi, and C.-R. Ji, Phys. Rev. D **63**, 074014 (2001).

[36] P. Maris and C. D. Roberts, Phys. Rev. C **56**, 3369 (1997).

[37] V. A. Karmanov and J. Carbonell, Eur. Phys. J. A **27**, 1 (2006); J. Carbonell and V. A. Karmanov, Eur. Phys. J. A **27**, 11 (2006).

[38] S. J. Brodsky, C.-R. Ji, and M. Sawicki, Phys. Rev. D **32**, 1530 (1985).

[39] W. Jaus, Phys. Rev. D **41**, 3394 (1990).

[40] S. J. Brodsky and J. R. Primack, Ann. Phys. (N.Y.) **52**, 315 (1969), and references therein.

[41] F. Coester and D. O. Riska, Ann. Phys. (N.Y.) **234**, 141 (1994).

[42] D. Lurié, A. J. Macfarlane, and Y. Takahashi, Phys. Rev. **140**, B1091 (1965).

[43] T. Frederico, H.-C. Pauli, and S.-G. Zhou, Phys. Rev. D **66**, 054007 (2002); **66**, 116011 (2002).

[44] J. P. B. C. de Melo, T. Frederico, E. Pace, G. Salmé, and J. S. Veiga, in *Proceedings of the Workshop on "Continuous Advances in QCD", Minneapolis* (World Scientific, Singapore, 2007), p 525.

[45] C.-R. Ji and H.-M. Choi, Phys. Lett. B **513**, 330 (2001).

[46] P. A. M. Dirac, Rev. Mod. Phys. **21**, 392 (1949).

[47] P. L. Chung, F. Coester, and W. N. Polyzou, Phys. Lett. B **205**, 545 (1988).

[48] F. Schlumpf, Phys. Rev. D **50**, 6895 (1994).

[49] J. P. B. C. de Melo, T. Frederico, E. Pace, S. Pisano, and G. Salmè, Phys. Lett. B **671**, 153 (2009).

[50] G. A. Miller, Phys. Rev. C **79**, 055204 (2009).

[51] D. Brömmel *et al.*, Eur. Phys. J. C **51**, 335 (2007).

[52] R. Baldini *et al.*, Eur. Phys. J. C **11**, 709 (1999); Nucl. Phys. **A666-A667**, 38 (2000); (private communication).

[53] J. Volmer *et al.*, Phys. Rev. Lett. **86**, 1713 (2001).

[54] J. A. O. Marinho, T. Frederico, E. Pace, G. Salmè, and P. U. Sauer, Phys. Rev. D **77**, 116010 (2008).

[55] D. Brömmel *et al.* (QCDSF/UKQCD Collaboration), Proc. Sci., LAT2005 (2005) 360; LATTICE2007 (2007) 140;D. Brömmel, Report No. DESY-THESIS-2007-023, 2007.

[56] D. Brömmel *et al.*, Phys. Rev. Lett. **101**, 122001 (2008).

[57] T. Frederico, E. Pace, S. Pisano, and G. Salmè, arXiv:0802.3144.

[58] D. Amrath, M. Diehl, and J. P. Lansberg, Eur. Phys. J. C **58**, 179 (2008).

[59] T. Frederico, E. Pace, and G. Salmè (to be published).